AD NUMBER

AD237931

LIMITATION CHANGES

TO:

Approved for public release; distribution is unlimited.

FROM:

**Distribution authorized to U.S. Gov't. agencies and their contractors;
Administrative/Operational Use; 25 APR 1960.
Other requests shall be referred to Bureau of Ordnance, Department of the Navy, Washington, DC 20350.**

AUTHORITY

BUORD per APL ltr dtd 19 Jan 1966

This information is furnished upon the condition that it will not be released to another nation without specific authority of the Department of Defense of the United States, that it will be used for governmental purposes only, that individual or corporate rights originating in the information, whether patented or not, will be respected, and that the information be provided substantially the same degree of protection afforded it by the Department of Defense of the United States

ARPA Order No. 22-59
TASK 5

TG 331-4
Copy No.

TASK R

Quarterly Progress Report No. 4
for the period
1 January -- 31 March, 1960

TASK R IS A PROGRAM OF RESEARCH IN BASIC PHENOMENA ASSOCIATED WITH THE BEHAVIOR OF MATERIALS IN HIGH TEMPERATURE GAS ENVIRONMENTS. IT IS SUPPORTED BY THE ADVANCED RESEARCH PROJECTS AGENCY THROUGH CONTRACT NORD 7386 WITH THE BUREAU OF NAVAL WEAPONS, DEPARTMENT OF THE NAVY.

THE JOHNS HOPKINS UNIVERSITY
APPLIED PHYSICS LABORATORY
8621 GEORGIA AVENUE SILVER SPRING, MARYLAND

ARPA Order No. 22-59
TASK 5

TG 331-4
April 25, 1960

TASK R

Quarterly Progress Report No. 4
for the period
1 January – 31 March, 1960

THE JOHNS HOPKINS UNIVERSITY
APPLIED PHYSICS LABORATORY
8621 GEORGIA AVENUE SILVER SPRING, MARYLAND

GENERAL OBJECTIVES OF TASK R

Many of the wide variety of problems associated with the use of materials at high temperatures occur in connection with advanced propulsion systems, and of these, some of the most critical and complex are encountered in high performance rocket motors. Present trends in rocket design and propellant formulation resulting in gas flows of increased temperature, pressure, and corrosiveness may be expected to aggravate the materials situation. It seems self-evident that future, long-range solutions to these problems must rely on more sophisticated approaches and broader knowledge of the behavior of materials in high temperature gas environments than is characteristic of the usual "quick-fix", or expensive cut-and-try test/procedures. It also seems likely that improvement in structural materials themselves (i.e., higher strength at high temperature, higher melting point, etc.) has reached the point of diminishing returns, so that various other subterfuges must be tried.

Research performed under Task R at the Applied Physics Laboratory or its subcontracting agencies is intended to provide some of the fundamental knowledge necessary for a rational understanding of the behavior of materials at high temperatures. This is a very broad and very complex field involving many different scientific disciplines. While no attempt is made to rigidly limit the scope of Task R, the general emphasis is on appropriate research in the flow and physical chemistry of high temperature gases such as are characteristic of advanced solid propellant rocket motors, and the phenomena basic to heat transfer and cooling techniques in such environments, rather than in the properties of materials themselves.

A. A. Westenberg
Program Coordinator

SUMMARY

I. High Temperature Chemical Kinetics in Laminar Flames ..... Page 1

The approach taken in this project is to obtain high temperature chemical kinetic information by means of the detailed analysis of laminar flame structure. Data on a CH_4-O_2 flame at 1/20 atm. pressure have been obtained and are compared with previous data on the same system at 1/10 atm. From this comparison it is demonstrated that the flame reactions are predominantly bimolecular. After careful study of all the conceivable elementary reactions which might occur, the simplest set which accounts for most of the observations is presented. Rate constants for the CO-OH and CH_4-OH reactions derived from the data and the assumed mechanism are shown to be reasonable and in fair agreement with other work. An over-all kinetic approach to the CO oxidation reaction is discussed.

II. Thermal Conductivity of Gases by a New Technique ..... Page 15

Extension of a method previously developed at APL for the accurate measurement of high temperature molecular diffusion coefficients to the measurement of thermal conductivity is being explored. Results with room temperature N_2 and He using an intermittent "off-on" line heat source are given. A high temperature furnace and associated equipment was constructed. Various methods of determining the radiation correction to the line source were considered.

III. Transport Properties in Dissociated Gases .....Page 20

Methods of measuring diffusion coefficients and thermal conductivity in gases composed of labile atoms and their parent molecules are being studied. The technique of measuring relative oxygen atom concentration by monitoring the light intensity caused by adding a trace of NO to an O-O_2 mixture is being used. Results of applying this technique in a flow-tube-with-a-side-arm apparatus show considerable promise of yielding good, absolute values for $D_{O\text{-}O_2}$. Both steady-state and transient experiments are reported. The effect of pressure, concentration, and side-arm counterflow velocity are shown to be in agreement with the theoretical model.

IV. High Temperature Chemical Kinetics from a Reacting Point Source... Page 30

The idea in this project is to derive over-all kinetic data by analyzing the concentration wake downstream of a point source trace gas injected into a laminar flow of a second gas with which it reacts. Difficulties have been encountered in

using CO as a tracer in O_2 because of disproportionation of CO on the metal injection tube and clogging of the latter by the carbon formed. Attempts are being made to try out the method with H_2 instead of CO, and some preliminary results are given.

V. Rocket Nozzle Fluid Dynamics ..... Page 34

This project aims at careful experimental measurements of the flow properties in a rocket nozzle employing a typical solid propellant. Pitot pressure surveys in the 12.5° total angle nozzle were in good agreement with equilibrium flow calculations, which was not the case with previously reported data for a 26° nozzle. This may be a result of the longer transit time available to a given area expansion in the smaller divergence nozzle. A number of test results with the infrared spectrometer used to determine gas composition in the nozzle are given, and equipment modifications described. The two-color ratio pyrometer used to measure surface temperatures in the nozzle is discussed in detail.

VI. Study of Condensed Phase-Vapor Equilibria ..... Page 48

The object of this work is to study the equilibria between condensed metal oxides and typical gas phase combustion products. A system of detecting the onset of condensation in the hot gas of a flat flame burner by means of light scattering is described. B_2O_3 in a H_2-O_2-N_2 flame is being studied first.

AAW/ccl

I. HIGH TEMPERATURE CHEMICAL KINETICS IN LAMINAR FLAMES

(R. M. Fristrom, C. Grunfelder, S. Favin, A. A. Westenberg)

Objective

The effect of chemical reactions is one of the important problems in the dynamics of high temperature, high speed gas flow. Chemistry and aerodynamics (and sometimes molecular transport processes) are strongly coupled in various nozzle flow and boundary layer phenomena. Advances in understanding in these areas cannot be made without a great deal more knowledge of high temperature chemical kinetics than is presently available. The important reactions are extremely rapid and lie in temperature regions where materials present problems. Therefore, conventional experimental techniques are not generally applicable, and the extrapolation of information from lower temperature reaction rate studies is not satisfactory. Several experimental techniques have been devised to surmount these difficulties. Shock tube studies are useful for very simple reaction systems. Molecular beam studies of chemical kinetics (inelastic scattering) are in their infancy, but offer interesting and exciting possibilities. The approach taken in this project is to study high temperature kinetics by a detailed quantitative analysis of laminar flame structure. From this analysis it is hoped that eventually the kinetics of elementary combustion reactions can be obtained. The present work allows the determination of the rates of appearance or disappearance of all of the stable species in a flame as a function of position (or time), temperature, and chemical composition. This is the same type of data obtained in conventional kinetic studies, and a much wider temperature range is accessible.

Experimental Techniques

The experimental techniques used to obtain the temperature, composition, and aerodynamic profiles through laminar flame zones are described in Ref. 1.

Analysis of the 1/20 Atmosphere CH_4-O_2 Flame

The experimental data obtained in a 1/20 atm. flat CH_4-O_2 flame of the same initial composition ($X_{CH_4} = 0.0785$; $X_{O_2} = 0.914$) as used previously at 1/10 atm. were analyzed during this report period. The procedure was exactly as described in previous reports (Refs. 2,3). Atom and enthalpy balances were satisfactory to about the same degree as before. Since these offer nothing new they are not shown here.

It is of considerable interest to compare the structural data derived from the two flames. An instructive example is provided by the two temperature profiles. As can be shown theoretically (Ref. 4), if all the reactions involved in a flame are of order n, all distances should be proportional to $P^{-n/2}$. Thus if most of the important reactions are second order, as seems likely, the distance coordinate in the flame should be an inverse function of P. In the present case, the two flames were studied at pressures differing by a factor of two, so that a given profile in the 1/10 atm. flame should be compared with its counterpart in the 1/20 atm. flame plotted with its distance coordinate halved. This comparison is shown in Fig. I-1. The circled points are the direct experimental data for the 1/10 atm. flame and the triangular points are the 1/20 atm. data plotted against z/2. (The latter were also translated downstream somewhat after halving to show the congruence of the two curves.)

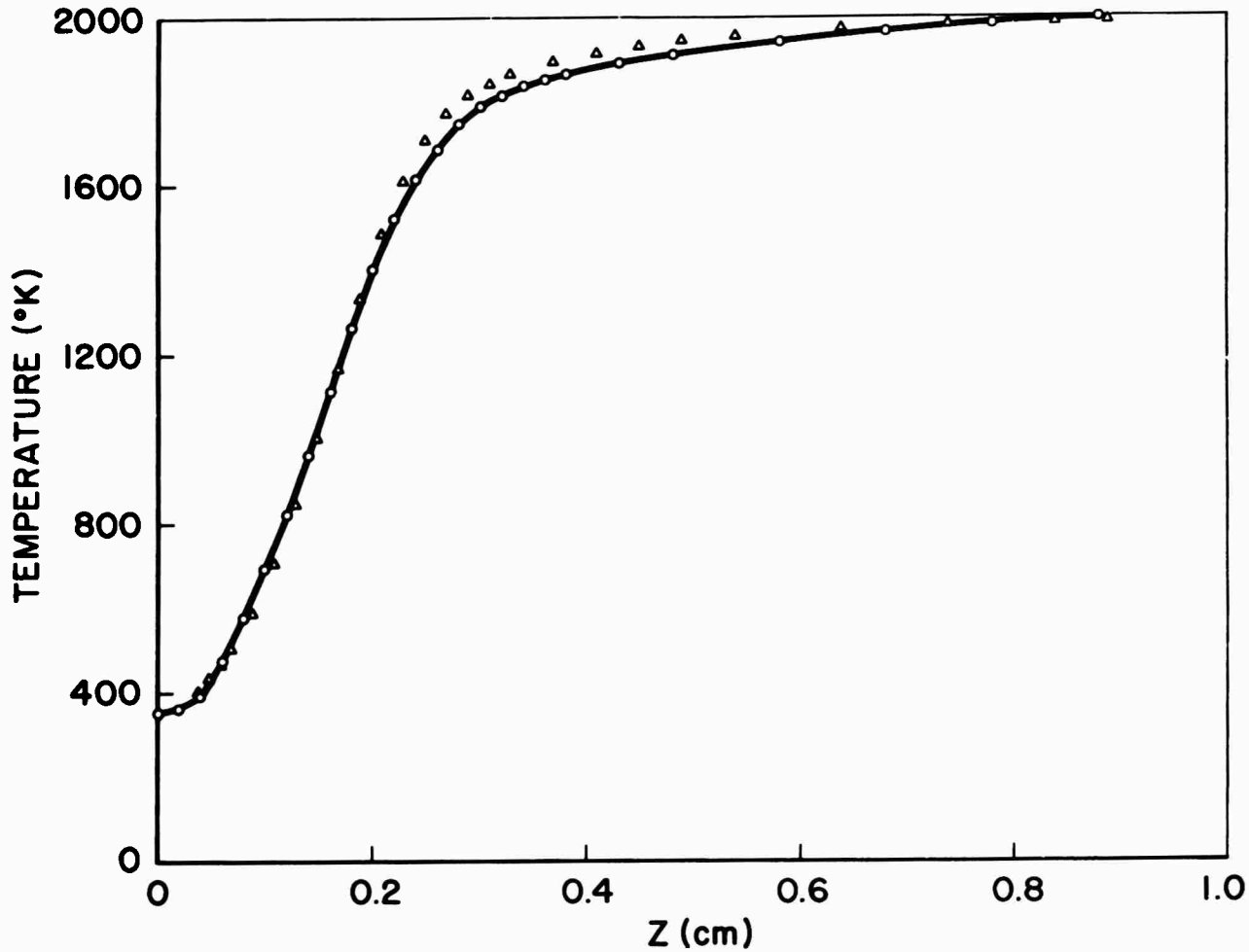

Fig. I-1 PLOT SHOWING CONGRUENCE OF THE CH_4-O_2 FLAME TEMPERATURE PROFILES AT TWO PRESSURES

O : Data for 1/10 atm. flame
Δ : Data for 1/20 atm. flame plotted against Z/2

The similarity in shape is strikingly apparent, and this provides support for the postulate of there being predominantly second order reactions in the flame. Plots of the composition variables show similar congruence for the two flames. Fig. I-2 shows the case of X_{H_2O}.

Chemical Kinetic Considerations

The net rates of reaction per unit volume K_i were computed for the stable species of the 1/20 atm. flame as before (Ref. 3). The general appearance of the rate curves is similar to the 1/10 case. In both flames there is an initial region where all changes in variables are due only to molecular transport, a fast reaction region setting in at a temperature of about 1300°, and then a wide afterburning region where CO is converted to CO_2.

As previously pointed out (Ref. 3), the K_i curves may be checked against each other by making use of the conservation of individual chemical elements. Thus conservation of carbon leads to

$$K_{CO} = -K_{CH_4} - K_{CO_2} - K_{H_2CO} \qquad (1)$$

and of hydrogen

$$K_{H_2O} = -2K_{CH_4} - K_{H_2} - K_{H_2CO} \qquad (2)$$

neglecting free radical contributions. The experimental 1/20 atm. rates are compared according to these equations in Figs. I-3 and I-4. The agreement is somewhat better than it was for the 1/10 atm. flame.

Another comparison of some significance is afforded by the rate profiles of a given species in the two flames. Consider the case of K_{H_2O}. If we assume that the net rate of water formation at any point is predominantly due to second

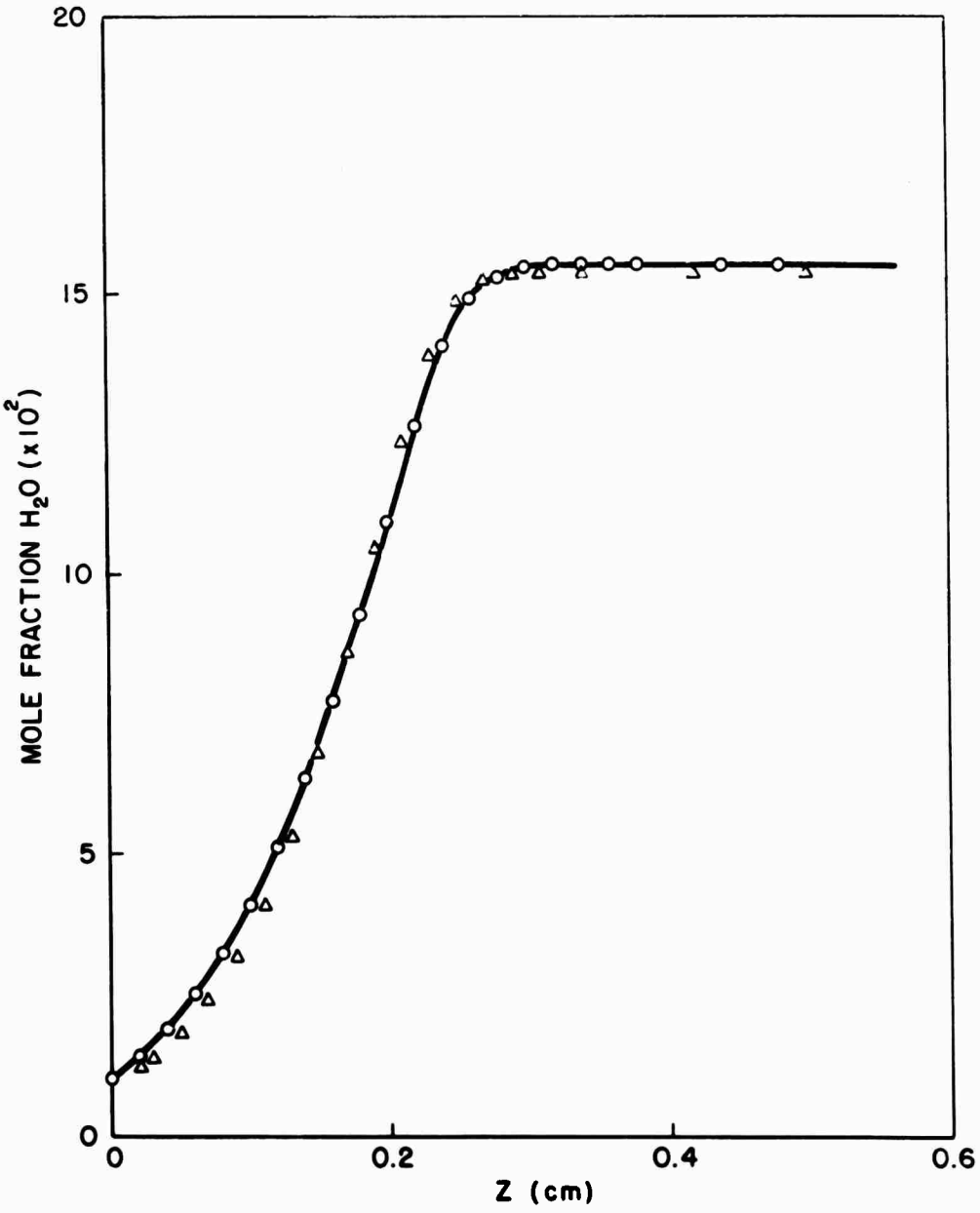

Fig. I-2 PLOT SHOWING CONGRUENCE OF THE WATER MOLE FRACTION PROFILE IN THE CH_4-O_2 FLAME AT TWO PRESSURES

O : Data for 1/10 atm. flame
Δ : Data for 1/20 atm. flame plotted against Z/2

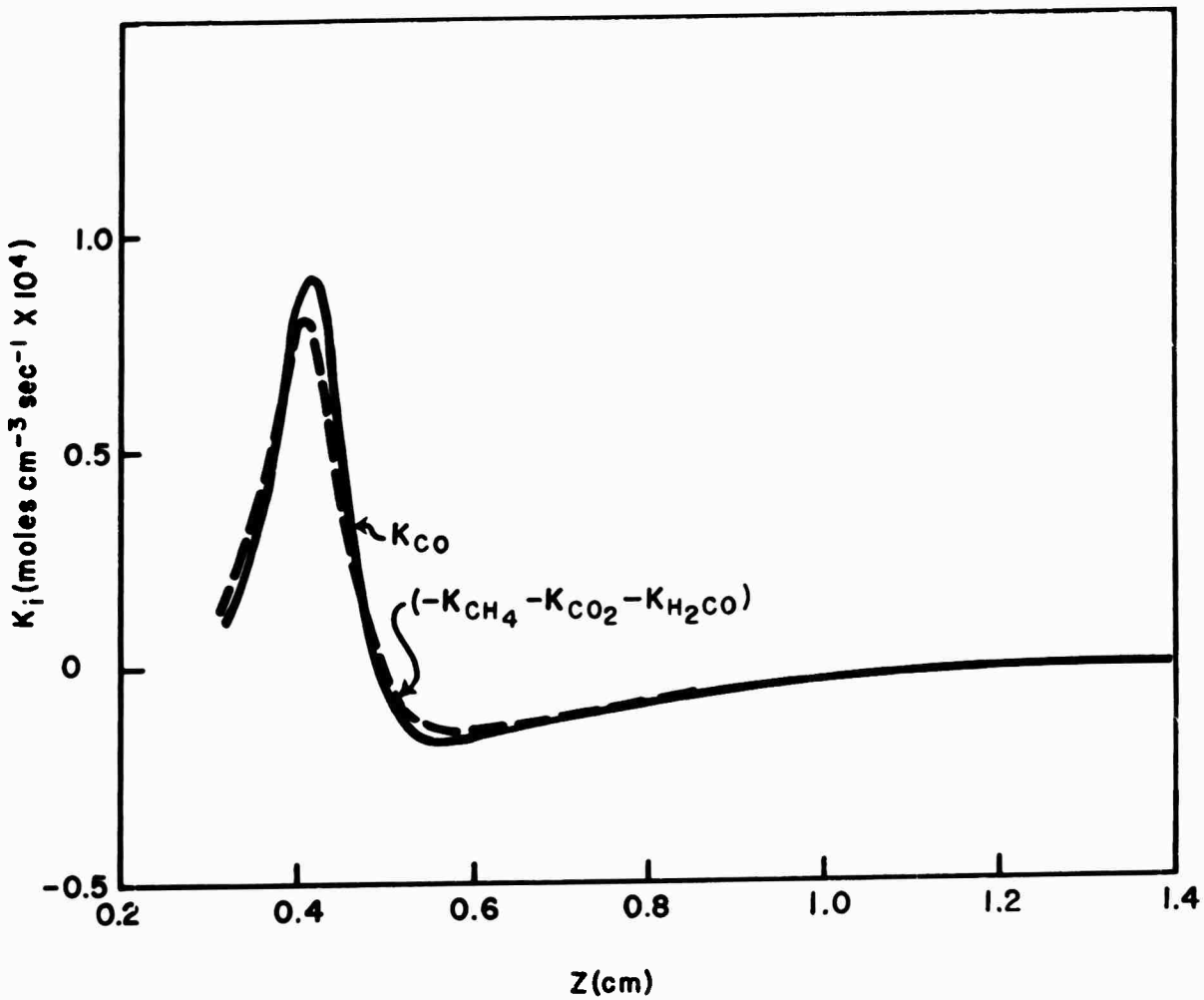

Fig. I-3 COMPARISON OF K_{CO} WITH THE COMBINED RATE $(-K_{CH_4} - K_{CO_2} - K_{H_2CO})$ Pressure = 1/20 atm.

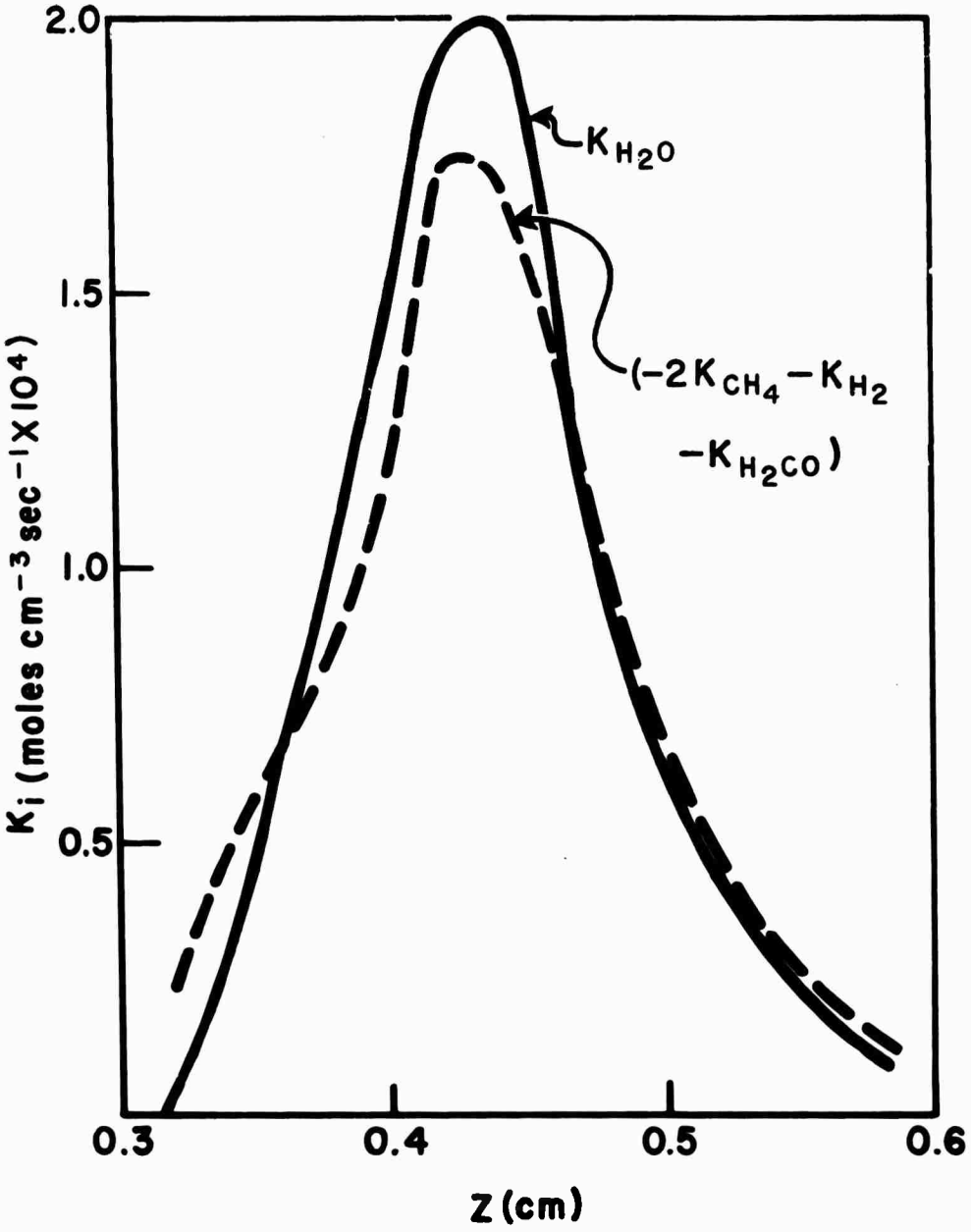

Fig. I-4 COMPARISON OF K_{H_2O} WITH THE COMBINED RATE $(-2K_{CH_4} - K_{H_2} - K_{H_2CO})$ Pressure = 1/20 atm.

order reactions, we can write in general

$$K_{H_2O} = \frac{P^2}{(RT)^2} \sum_J k_J (X_i X_j)_J \qquad (3)$$

where k_J is the rate constant of the Jth reaction involved in H_2O formation (or destruction - negative k_J), P, R and T have their usual meanings, and the $(X_iX_j)_J$ signifies the mole fraction product of whatever species enter into the Jth reaction. It will be noted from this equation that, in comparing flames at different pressures, if the temperature and mole fraction profiles are congruent when plotted on the proper distance scale (i.e., $z \propto P^{-1}$ in this case, as previously discussed), then the rate profiles should be compared keeping in mind that $K_i \propto P^2$. The comparison for K_{H_2O} is shown in Fig. I-5. Solid curve A is the K_{H_2O} profile for the 1/10 atm. flame. Solid curve B is the K_{H_2O} profile for the 1/20 atm. flame plotted against z/2 (and somewhat translated). The dotted curve C is the K_{H_2O} for the 1/20 atm. flame multiplied by 4 to account for the pressure difference between the two flames. The general agreement is remarkable. While it has not been possible to show that all the mole fraction profiles for the species (unknown at this point) entering into the net formation of H_2O are congruent in the two flames, the fact that temperature, X_{H_2O}, and K_{H_2O} are congruent makes it very likely that they are, and lends considerable credence to the second order reaction hypothesis. The comparisons for other K_i show similar results when plotted on a P^2 basis.

The actual mechanism of reaction in the methane-oxygen system has been investigated many times by others using varying techniques and conditions. Most of these have been summarized by Lewis and von Elbe (Ref. 5) and Semenov (Ref. 6). Almost all the previous work, however, was done at lower temperatures

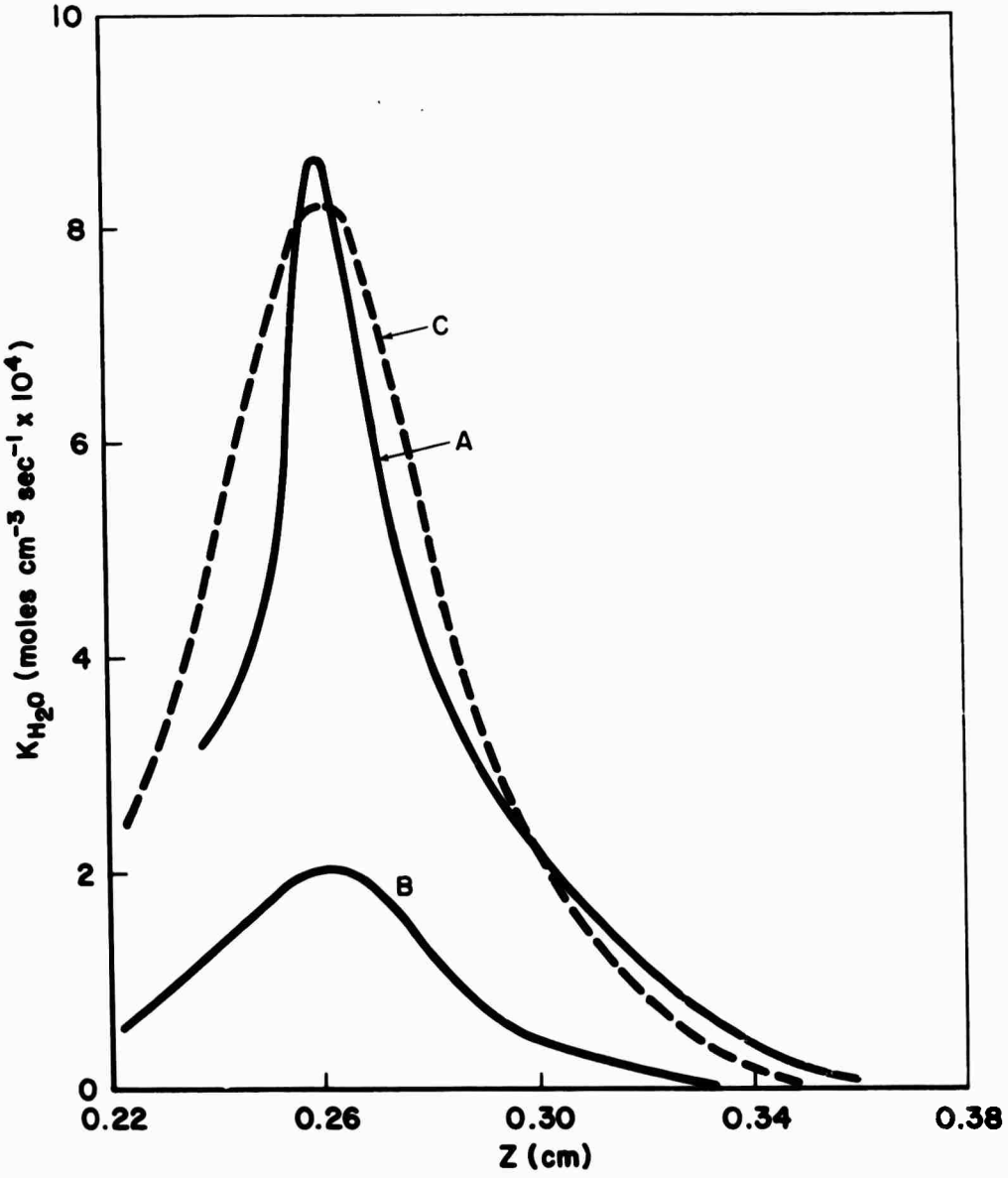

Fig. I-5 PLOT SHOWING CONGRUENCE OF NET FORMATION RATE OF WATER IN THE CH_4-O_2 FLAME AT TWO PRESSURES

A: K_{H_2O} for 1/10 atm. flame

B: K_{H_2O} for 1/20 atm. flame plotted against Z/2

C: K_{H_2O} for 1/20 atm. flame plotted against Z/2 and multiplied by 4

than those characteristic of the present flames, and under conditions where wall effects were likely to be of importance. An exception is the recent work of Fenimore and Jones (Ref. 7) also done in a laminar flame. In any case, we have spent considerable time during this quarter examining anew all of the conceivable elementary reactions which might occur in the flames. The only restrictions were that just reactions involving common, simple species were considered, so that practically all of the many peroxides, aldehydes, etc. which have been postulated as intermediates in such systems were rejected as being so thermally unstable or inherently unlikely as to be of negligible importance. Also, termolecular reactions were eliminated (except for the usual radical or atom recombination processes) as being too improbable at these pressures compared to bimolecular reactions to contribute to the main features of the flame kinetics. The list of possible reactions was then carefully gone over and many of them eliminated on the basis of energetics, steric improbability, concentration, or violation of spin conservation rules (i.e., low transmission coefficient).

The result of this study was the following proposed mechanism which seems to account for most of the observations:

I. $CH_4 + OH \underset{k_2}{\overset{k_1}{\rightleftharpoons}} CH_3 + H_2O$

II. $CH_4 + O \longrightarrow CH_3 + OH$

} Methane disappearance
Water formation

III. $CH_3 + O_2 \xrightarrow{k_3} H_2CO + OH$ (two steps)

IV. $H_2CO + OH \xrightarrow{k_4} HCO + H_2O$

V. $HCO + OH \xrightarrow{k_5} CO + H_2O$

} Intermediate formation
Water formation

VI. $CO + OH \xrightarrow{k_6} CO_2 + H$ — Carbon dioxide formation

VII. $H + O_2 \xrightarrow{k_7} OH + O$

VIII. $H + H_2O \xrightarrow{k_8} OH + H_2$ — Radical removal

IX. $O + O + M \xrightarrow{k_9} O_2 + M$ — Hydrogen formation

X. $OH + OH \xrightarrow{k_{10}} H_2O + O$

It will be seen that most of the activity is attributed to OH radical. The concentration of H atoms is kept very low by the large excess of O_2 and H_2O by way of reactions VII and VIII. O atom activity is largely restricted to probable participation in the disappearance of CH_4 in reaction II. The calculated final burned gas composition for the two flames is given in Table 1.

Table 1

Calculated final gas composition at hot boundary (T=2000°K)

Species	Mole Fractions	
	1/10 atm.	1/20 atm.
H_2O	0.15473	0.15349
CO_2	0.08022	0.07918
O_2	0.75273	0.75612
CO	0.00040	0.00056
H_2	0.00016	0.00023
N_2	0.00060	0.00060
NO	0.00042	0.00042
A	0.00340	0.00018
OH	0.00528	0.00626
O	0.00201	0.00285
H	0.00007	0.00011

The distribution of OH radicals in the flame may be computed from the rate data by making use of reaction VI, since according to the assumed mechanism, this is the only contribution to the net rate of CO_2 formation. In view of the probability that the H atom concentration is very low, the reverse of VI has not been included. Thus we can write

$$K_{CO_2} = k_6 \, N^2 \, X_{CO} \, X_{OH} \qquad (4)$$

where N is the total molar density. If we now fit our experimental K_{CO_2} data to Eq. (4) at the hot boundary by assuming that X_{OH} is the computed equilibrium value (a reasonable assumption), we can obtain a value of k_6 since the other quantities in Eq. (4) are known. In this way we get

$$k_6 \ (1980^\circ) = 1 \times 10^{12} \ cm^3 mole^{-1} sec^{-1} \ (1/10 \ atm.)$$

$$k_6 \ (1990^\circ) = 0.3 \times 10^{12} \ cm^3 mole^{-1} sec^{-1} \ (1/20 \ atm.)$$

Since the temperatures are essentially the same, ideally these two values should agree. We may take an average value of the two and use 0.6×10^{12} as the experimental k_6 at about $2000^\circ K$.

The rate constant can be put in the simple Arrhenius form

$$k_6 = A_6 \exp(-E_6/RT) \ . \qquad (5)$$

The activation energy E_6 has been estimated by Avromenko and Lorentso (Ref. 8) to be 7 kcal/mole, and by Fenimore and Jones (Ref. 9) to be about 10 kcal/mole. The pre-exponential frequency factor A_6 (assumed constant) has been estimated by the same authors as 3×10^{12} and 2.3×10^{13} $cm^3 mole^{-1} sec^{-1}$, respectively. From our average value of k_6 at 2000°, we get $A_6 = 3.5 \times 10^{12}$ using $E_6 = 7$, and $A_6 = 8 \times 10^{12}$ using $E_6 = 10$. These are in reasonable agreement with the results

of the other authors - somewhat closer to those of Ref. 8. The low value of the activation energy implies that the rate constant is practically independent of temperature, of course.

Using the expression for k_6 derived in this way for the 1/10 atm. flame, for example, it is now possible to compute an OH concentration profile through the flame zone by means of Eq. (4). The result of this computation is given in Fig. I-6. It will be noted that X_{OH} is nearly constant in the latter part of the flame where the only reaction of importance is the conversion of CO to CO_2 (presumably by VI), but rises to a maximum in the region immediately downstream of the fast reaction zone. This general behavior of radicals in flames has been commented on many times in the past - mostly on the basis of theoretical studies. It is typical of species formed as an intermediate whose concentration at both hot and cold boundaries is nearly zero. Experimentally, radical concentrations in the burned gas of hydrocarbon-air and hydrogen-air flames have been measured by an isotope labeling technique by Fenimore and Jones (Ref. 10) and spectroscopically by Kaskan (Refs. 11, 12) and Bulewicz, James, and Sugden (Ref. 13). The general conclusions of these studies have been that radical concentrations (H and OH) may be two or three orders of magnitude above equilibrium values in rich hydrogen flames, several times greater than equilibrium in lean hydrogen flames, and essentially the equilibrium value in hydrocarbon flames. (The latter conclusion supports our use of the equilibrium OH concentration in computing k_6.) In the present case, Fig. I-6 shows $(X_{OH})_{max}$ occurring at z = 0.3 cm where the temperature is 1750°K. The ratio $(X_{OH})/(X_{OH})_{equil}$ at this point is about 10, which seems reasonable in view of the above results.

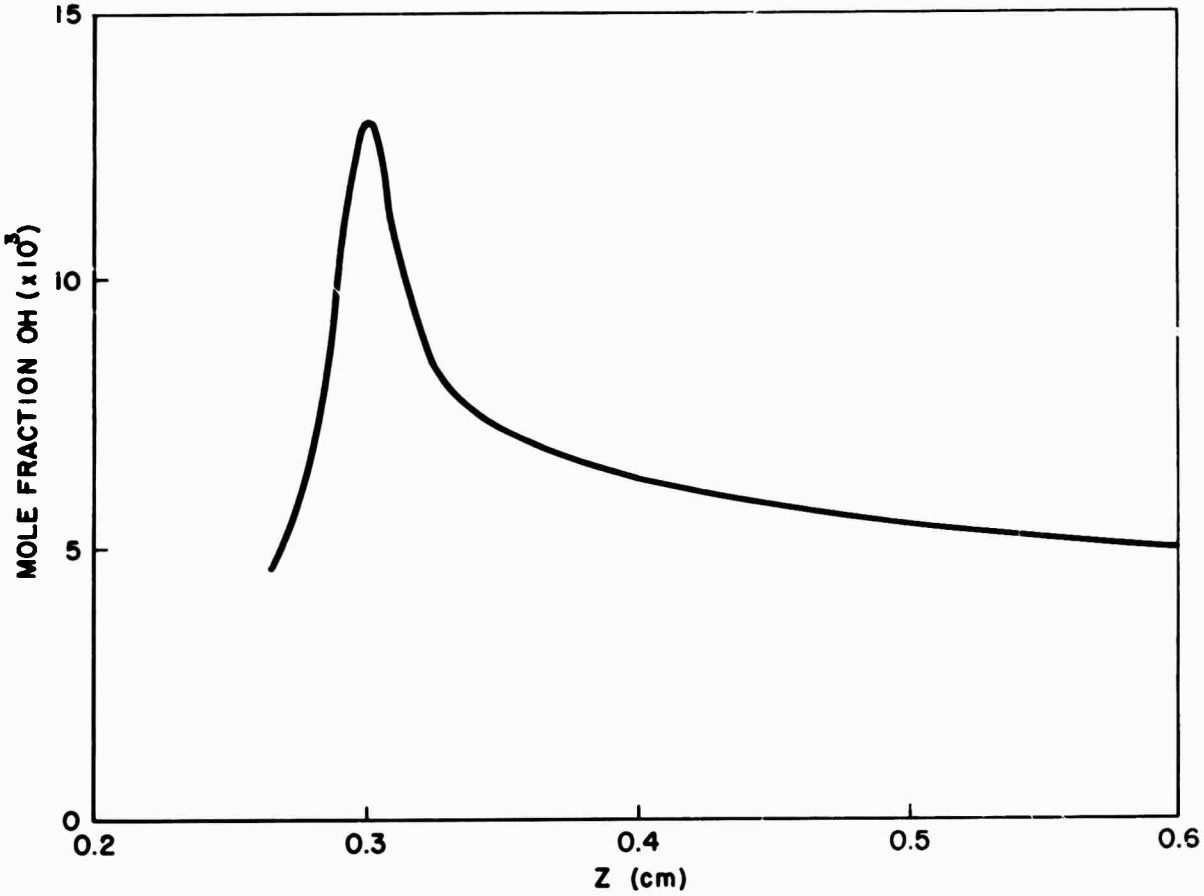

Fig. I-6 MOLE FRACTION PROFILE OF OH RADICAL IN 1/10 ATM. FLAME - FITTED TO EQUILIBRIUM CONCENTRATION AT HOT BOUNDARY

The disappearance of CH_4 in the flame has been attributed to OH radicals and/or O atoms by way of reactions I and II. Which of these - if either one - is more important is not possible to state for sure at this time. In view of the fact that the final equilibrium concentration of OH is more than twice that of O (see Table 1), and that there are more sources of OH radicals than of O atoms in the proposed mechanism, it seems likely that reaction I would be more important. (Presumably the reaction II could not occur in any given situation without I occurring also, since II generates OH radicals, but the converse would not be true.) If we neglect the possibility of CH_4 + O reaction for the moment, the OH profile obtained from the CO_2 production rate may be used to obtain a rate constant for I. Thus we can write

$$K_{CH_4} = - k_1 N^2 X_{CH_4} X_{OH} \qquad (6)$$

Solving for k_1 from the experimental data gives values (using X_{OH} profiles individually fitted at the hot boundary of each flame)

$$k_1 \ (1650^\circ - 1790^\circ K) = 3 \times 10^{13} \ cm^3 mole^{-1} sec^{-1} \ (1/10 \ atm.)$$

$$k_1 \ (1660^\circ - 1840^\circ K) = 1 \times 10^{13} \ cm^3 mole^{-1} sec^{-1} \ (1/20 \ atm.)$$

Over the temperature range in the flame where both K_{CH_4} and X_{OH} data were available, k_1 was independent of temperature in both cases. The only available estimate of E_1 is about 8.5 kcal/mole (quoted in Ref. 6). Over the temperature range 1650°-1840° the factor exp (-8500/RT) varies only from 0.08 to 0.10, which is well within the scatter of the k_1 values determined, so that such a small temperature dependence would not be detectable. The point really is that a k_1 value of about 2×10^{13} is entirely reasonable. Taken by itself this would imply a steric factor about 10 times larger than that for reaction VI (the

activation energies are probably roughly equal). This may be sensible in view of the spherical symmetry of the CH_4 molecule. If part of the measured CH_4 disappearance rate is due to O atoms, however, the estimate of k_1 obtained by assuming it is all due to OH reaction would be too high, which would tend to overestimate the steric factor of reaction I.

It should be noted that Fenimore and Jones (Ref. 7) rule out reaction I as an important reaction in methane flames on the basis of indirect arguments involving the relative rates of H_2O and CO_2 formation in near-stoichiometric CH_4-H_2-O_2-A flames. Since (as far as we can tell) they made no actual measurements of H_2O concentration, we do not regard their argument as very convincing.

Finally, some comments on over-all kinetics in connection with these results are in order. In the previously quarterly report (Ref. 3) it was pointed out that one could write as an empirical expression

$$K_{CO_2} = k\, N^2\, X_{CO}\, X_{O_2} \qquad (7)$$

which says nothing about the actual mechanism of CO-CO_2 conversion, but may be useful as a practical kinetic relation. It was shown that the 1/10 atm. data gave a value of $k \sim 8 \times 10^9$ $cm^3 mole^{-1} sec^{-1}$ which was temperature-independent in the range 1650-1940°K. Fairly good agreement was shown with the work of other investigators similarly interpreted. The 1/20 atm. flame data yield a value of $k \sim 7 \times 10^9$. Since the X_{O_2} was the same in both flames, the good agreement indicates that the N^2 (i.e., P^2) dependence of the K_{CO_2} assumed in (7) must be correct.

Since it is suspected that the actual mechanism of CO disappearance is via reaction with OH in VI, the question arises as to why a relation like Eq. (7)

seems to give a good correlation of quite a wide variety of flame results. In view of the known influence of H_2O on the CO-CO_2 reaction, Eq. (7) has been presumed to hold only in presence of considerable H_2O. It would be interesting if one could show that X_{OH} is proportional to X_{O_2} in such a case, which would put Eq. (7) on a firmer basis. Actually, if one regards the CO afterburning part of the flame as a region where there is an equilibrium mixture of O_2, H_2O, OH, O, H, H_2 (the latter two species in very small concentrations in our case), then, in terms of the major components O_2 and H_2O, the OH concentration may be shown to be

$$X_{OH} = \frac{X_{H_2O}^{1/2} \; X_{O_2}^{1/4}}{K_A^{1/2} \; K_B^{1/4} \; P^{1/4}} \tag{8}$$

where K_A and K_B are the equilibrium constants (partial pressure units) for the reactions

$$\text{(A)} \quad OH + OH \rightleftharpoons H_2O + O \; ; \quad K_A = \frac{P_{H_2O} \; P_O}{P_{OH}^2}$$

$$\text{(B)} \quad O + O + M \rightleftharpoons O_2 + M \; ; \quad K_B = \frac{P_{O_2}}{P_O^2}$$

and P is the total pressure. Using Eq. (8) in Eq. (4) gives

$$K_{CO_2} = \frac{k_6 \; N^2}{K_A^{1/2} \; K_B^{1/4} \; P^{1/4}} \; X_{CO} \; X_{H_2O}^{1/2} \; X_{O_2}^{1/4} \tag{9}$$

as the expression for the CO_2 formation rate from CO reacting in an equilibrium (with respect to H_2O, O_2, H_2, H, and O) concentration of OH. This obviously is <u>not</u> a first-order dependence on X_{O_2} as assumed in Eq. (7). It is of considerable

interest to note, however, that the concentration dependences of the rate as given in Eq. (9) are precisely those found by Kozlov (Ref. 14) in a more-or-less conventional flow reactor experiment and stated by him as having been verified by several other Russian workers in various flame propagation (i.e., burning velocity) studies. Hence, it seemed possible that Eq. (9) might represent a usable over-all kinetic expression for CO burning in an equilibrium mixture containing excess O_2 and H_2O, and one which was more firmly based than Eq. (7). With this in mind, the present data were compared with those of the other flame studies available. For each case, the elementary rate constant k_6 was evaluated by means of Eq. (9), all the other factors being experimentally measured or standard available data. For the present flame data, of course, the values of k_6 were essentially the same as quoted earlier in this report, since those were obtained by the same hot boundary (equilibrium) assumption used in deriving Eq. (9). The results are given in Table 2.

Table 2. Comparison of rate-constants for the CO-OH reaction (equilibrium OH assumption) from work of various authors.

Author	Flame System	k_6 ($cm^3 mole^{-1} sec^{-1}$) x 10^{-12}
This work	CH_4-O_2 at 0.1 atm.	1.2 (1940°K)
	CH_4-O_2 at 0.05 atm.	1.0 (1940°K)
Friedman & Cyphers (Ref. 15)	C_3H_8-air at 0.06 atm.	2.1 (1600°K)
Friedman & Nugent (Ref. 16)	CO-O_2-H_2O at 0.04 atm.	0.7 (1800°K)
Fenimore & Jones (Ref. 17)	C_2H_2--air at 1 atm.	0.2 (1885°K)

The agreement between these values is considerably better than those shown previously (Ref. 3) using the assumption of Eq. (7). The improvement is especially pronounced for the first three studies at low pressure. Fenimore and Jones (Ref. 17) quote several other sets of data for flames having much less O_2 present, and values k_6 calculated from these are quite a bit lower than those in the table. It may be that the equilibrium OH assumption breaks down under these conditions. Indeed, Ref. 14 notes that the relation (9) holds only for oxygen concentrations greater than 5%.

- - - -

Two papers on the CH_4-O_2 flame studies were submitted to the Journal of Physical Chemistry during this quarter.

References

1. Task R Quarterly Progress Report No. 1, 1 April - 30 June 1959. The Johns Hopkins University, Applied Physics Laboratory Report No. TG-331-1 (July 1959).

2. Task R Quarterly Progress Report No. 2, 1 July - 30 Sept. 1959. The Johns Hopkins University, Applied Physics Laboratory Report No. TG-331-2 (October 1959).

3. Task R Quarterly Progress Report No. 3, 1 October - 31 December 1959. The Johns Hopkins University, Applied Physics Laboratory, Report No. TG-331-3 (January 1960).

4. J. O. Hirschfelder, C. F. Curtiss, and R. B. Bird, The Molecular Theory of Gases and Liquids, (John Wiley & Sons, Inc., New York, 1954) p. 765.

5. B. Lewis and G. von Elbe, Combustion, Flames and Explosions of Gases, (Academic Press, New York, 1951) Chap. IV.

6. N. N. Semenov, Some Problems in Chemical Kinetics and Reactivity, (Princeton University Press, Princeton, N. J., 1958) Vol. II, Chap. XII.

7. C. P. Fenimore and G. W. Jones, J. Phys. Chem. 63, 1834 (1959).

8. L. Avramenko and R. V. Lorentso, Zhur. Fiz. Khim. 24, 207 (1950).

9. C. P. Fenimore and G. W. Jones, J. Phys. Chem. 62, 1578 (1958).

10. C. P. Fenimore and G. W. Jones, J. Phys. Chem. 62, 693 (1958).

11. W. E. Kaskan, Combustion and Flame 2, 229 (1958).

12. W. E. Kaskan, Combustion and Flame 2, 286 (1958).

13. E. M. Bulewicz, C. G. James, and T. M. Sugden, Proc. Roy. Soc. A235, 89 (1956).

14. G. J. Kozlov, Seventh Symposium on Combustion, (Butterworths, London, 1959) p. 142.

15. R. Friedman and J. A. Cyphers, J. Chem. Phys. 23, 1875 (1955).

16. R. Friedman and R. G. Nugent, Seventh Symposium on Combustion, (Butterworths, London, 1959) p. 311.

17. C. P. Fenimore and G. W. Jones, J. Phys. Chem. 61, 651 (1957).

II. THERMAL CONDUCTIVITY OF GASES BY A NEW TECHNIQUE

(R. E. Walker, N. deHaas, A. A. Westenberg)

Objective

The analysis of the problem of convective heat transfer both in the laminar and turbulent flow regimes requires that the properties of the gases involved be quantitatively understood. The coefficient of thermal conductivity is one such property. Measurement of thermal conductivity of gases has not been a forsaken field of research, and several common gases have been investigated up to temperatures approaching reaction motor temperatures. The primary shortcomings of past and present research in the study of thermal conductivity of gases for application to such heat transfer problems are: a) inability to apply present experimental methods to temperatures above about 1000°K (most measurements are made at substantially lower temperatures than this, b) the complexity and difficulty in using the usual apparatus for this measurement (thermal-conductivity cells), and c) the lack of measurements on species (and mixtures) prevalent in reaction motors. Other shortcomings could be listed.

Recent measurements of molecular diffusion coefficients - a closely related transport property (Ref. 1) - of common flame gases at temperatures in excess of 1000°K applied a simple concept (Ref. 2) that could, in principle, be used for measuring other gas transport properties (conductivity and viscosity). In this method, a point source of a trace gas is located in the center of a uniform, heated laminar jet of a second gas. A series of gas samples removed immediately downstream of the source and quantitatively analyzed is used to determine the molecular diffusion coefficient. The technique has good precision ($\pm$1-2%) and is quite adaptable to high temperatures and various gas types.

Application of this method to the measurement of thermal conductivity of gases is an obvious extension. The source of trace gas is replaced with a point (or line) source of heat and the temperature rise downstream of the heat source is measured with an appropriate technique. The method is simple, should have good precision ($\pm 2\%$), and can be used with a variety of gases at high ambient temperature (approaching flame temperatures). Thus, the objective of this research is to employ the point-source or the line-source technique in the measurement of gas thermal conductivity and, if successful, to use the method for obtaining data over a wide range of temperature on pure gases and mixtures of propulsive interest.

Theory of the Method

This has been described in detail in Ref. 3.

Experimental Technique

The experimental technique of measuring the thermal conductivity of a gas using the line source is described in Ref. 4, with the alterations outlined in Ref. 5. For the "final" room temperature measurements presented in this report, a 1 mil Pt-10%Rh wire with potential taps was used with the "off-on" (square wave) heat source which was described in Ref. 5.

Room Temperature Thermal Conductivities of Nitrogen and Helium

Table 1 presents the results of the room temperature measurements for nitrogen and helium. Comparing the measured λ's with those obtained by others using conventional techniques it is seen that excellent agreement exists for these two cases which have widely different conductivities.

Table 1

Gas	q 10^3 cal/cm sec	U cm/sec	Re	$G^{1/3}$	T °K	λ 10^5 cal/cm sec °K [these measurements]	λ(Ref.) 10^5 cal/cm sec °K [other measurements]
N_2	7.54	40	.65	.054	300	6.28	6.24 (6)
N_2	10.83	40	.65	.058	300	6.24	6.24 (6)
He	13.71	130	.28	.0098	298	36.2	35.9 (7)

The Reynolds numbers (Re) and Grashof numbers to the one-third power ($G^{1/3}$) for the flow over the heat source wire are included to show in each case that (a) the Reynolds number is well below that for the onset of instabilities (Ref. 8), and (b) sufficiently large compared to $G^{1/3}$ so that the complicated effects of free convection (Ref. 9) are unimportant.

In all three measurements the thermal conductivities were obtained by applying the velocity wake correction which was described in Ref. 5. Also, a radiation correction of 1/2% was made of the q's for the two nitrogen runs. The helium run did not require such a correction. The results presented here are considered superior to those presented in Table II-1 of Ref. 5 because of the employment of the "off-on" heat source and because of care taken in obtaining proper alignment of the wire heat source with the thermocouple traversing mechanism. This is especially true for the helium run in which a significant zero drift was encountered.

High Temperature Measurements

During the period of this report a high temperature furnace with a line heat source was designed and constructed. It is constructed of inconel tubing which forms the inner lining of a wire-wound furnace on a ceramic tube.

The gas enters below the furnace and leaves at the top, which is open to receive the traversing differential thermocouple. It is believed that gas temperatures up to 1000°C may be obtained.

At elevated temperatures, a sizeable radiation correction will have to be made. In anticipation of this, various methods of determining the radiation heat loss from the wire are being investigated. One method (which would be difficult) involves the evacuation of the region about the heat source while duplicating the other conditions of a conductivity measurement. From several standpoints it would be more desirable if a radiation correction could be determined by measurements taken just prior to or just after the measurements of the temperature profile with all conditions as they exist during the run. Methods of accomplishing this are being investigated.

- - - - -

A note describing the line source technique and our experience with it to date was accepted for publication in The Physics of Fluids.

References

1. J. O. Hirschfelder, C. F. Curtiss, and R. B. Bird, The Molecular Theory of Gases and Liquids, (John Wiley & Sons, Inc., New York, 1954).

2. R. E. Walker and A. A. Westenberg, J. Chem. Phys. 29, 1139 (1958).

3. Task R Quarterly Progress Report No. 2, 1 July - 30 Sept. 1959, The Johns Hopkins University, Applied Physics Laboratory Report No. TG-331-2.

4. Task R Quarterly Progress Report No. 1, 1 April - 30 June 1959, The Johns Hopkins University, Applied Physics Laboratory Report No. TG-331-1.

5. Task R Quarterly Progress Report No. 3, 1 October - 31 December 1959, The Johns Hopkins University, Applied Physics Laboratory Report No. TG-331-3.

6. National Bureau of Standards Circular 564, Tables of Thermal Properties of Gases.

7. H. L. Johnston and E. R. Grilly, J. Chem. Phys. 14, 233 (1946).

8. L. S. G. Kovasznay, Proc. Roy. Soc. 198A, 174 (1949).

9. D. C. Collis and M. J. Williams, J. Fluid Mech. 6, 357 (1959).

III. TRANSPORT PROPERTY STUDIES IN DISSOCIATED GASES

(R. E. Walker and A. A. Westenberg)

Objective

Convective heat transfer from dissociated gases to a catalytic wall is significantly affected by the chemical kinetics, the nature of the catalytic surface, and the transport properties of the mixture. Although gas phase kinetics for dissociated gases have been studied separately in shock tube experiments, attempts to measure the catalytic nature of a surface have revealed that it is difficult to separate the catalytic effects from those due to diffusion. Until very recently (Ref. 1) no separate measurements of diffusion coefficients had been made, so that gross estimates of this transport property are generally required to obtain catalytic activity of various surfaces. Additional diffusion measurements for a variety of dissociated gases are desirable for this reason.

In addition, measurements of diffusion coefficients as a function of temperature is an excellent way of determining intermolecular forces between unlike molecules. For dissociated gases, the (labile) atom-(parent) molecule intermolecular forces could be obtained in this manner and subsequently be used to predict other related transport coefficients. (These intermolecular forces can be determined from first principles for only the simplest interactions (H-H, H-H_2, H-He).) Measurements of thermal conductivity and/or heat transfer coefficients in dissociated gases are also of considerable intrinsic and practical interest. The present project is aimed at exploring and using various methods of experimental measurement of transport properties in dissociated gases.

Experimental Technique

In the previous progress report (Ref. 2) various possible experimental methods for measuring diffusion coefficients of dissociated gases were proposed. All of these techniques have certain merits but are deceptively difficult to exploit because of the loss of atoms through recombination (mostly wall recombination at the low pressures), and the ultimate necessity of measuring at least relative atom concentrations.

Recently, Krongelb and Strandberg (Ref. 1) have reported measurements of $O\text{-}O_2$ diffusion coefficients obtained with a transient method that utilizes the gradients in atom concentration created by wall recombination. The results from their investigations are limited, however, and additional experiments along this line are certainly warranted. They used paramagnetic resonance absorption for the detection of atoms - a complex and difficult approach. Fortunately, Kaufman (Ref. 3) has thoroughly examined a simple method of measuring relative oxygen-atom concentration by using the chemistry associated with the air afterglow phenomenon. In this method, a trace of nitric oxide, NO, is added to a partially dissociated oxygen gas. Two reactions compete to destroy oxygen atom and to form nitrogen dioxide, NO_2. These are

$$O + NO \longrightarrow NO_2 + h\nu \qquad (1)$$

and

$$O + NO + M \longrightarrow NO_2 + M \qquad (2)$$

with rate constants k_1 and k_2, respectively. The third body, M, is necessary to remove some of the energy released in the formation of NO_2. Kaufman reports that reaction (2) is the more important of these two reactions in removing O atoms

at pressures above about .015 mm Hg. The NO is regenerated through the reaction

$$O + NO_2 \longrightarrow NO + O_2 \qquad (3)$$

which is claimed to be very fast. The concentration of NO thus remains constant and the situation is therefore unique in that NO serves as an indicating catalyst for oxygen atoms, i.e., the luminosity of the yellow-green afterglow due to (1) is directly proportional to O .

During this report period, we have examined in some detail the ramifications of using NO as an O-atom indicator with the results reported below. They are in very good agreement with those reported by Kaufman. In addition, the experiments of Krongelb and Strandberg have been repeated using this method of measuring relative atom concentrations. Finally, a modified version of the counterflow method discussed in the previous progress report (Ref. 2) has been experimentally explored for the $O\text{-}O_2$ system using NO as an indicating catalyst. This has demonstrated distinct advantages over the transient method. The results from these preliminary experiments are also presented.

Quantitative Behavior of Using NO as an Indicating Catalyst for O Atoms

The experimental arrangement used to study the behavior of NO as an O-atom indicator is schematically shown in Fig. III-1. Oxygen atoms were produced by passing the gas through an electrodeless R.F. discharge powered by a 90-watt radio transmitter (EICO Model 720) operating at a frequency of 28 mc. A trace flow of NO was added to the gas-discharge products. Light intensity measurements were obtained with a 931A photomultiplier enclosed in a light-tight box through which the (dead-ended) side arm passed; a light sample 1 cm thick was used.

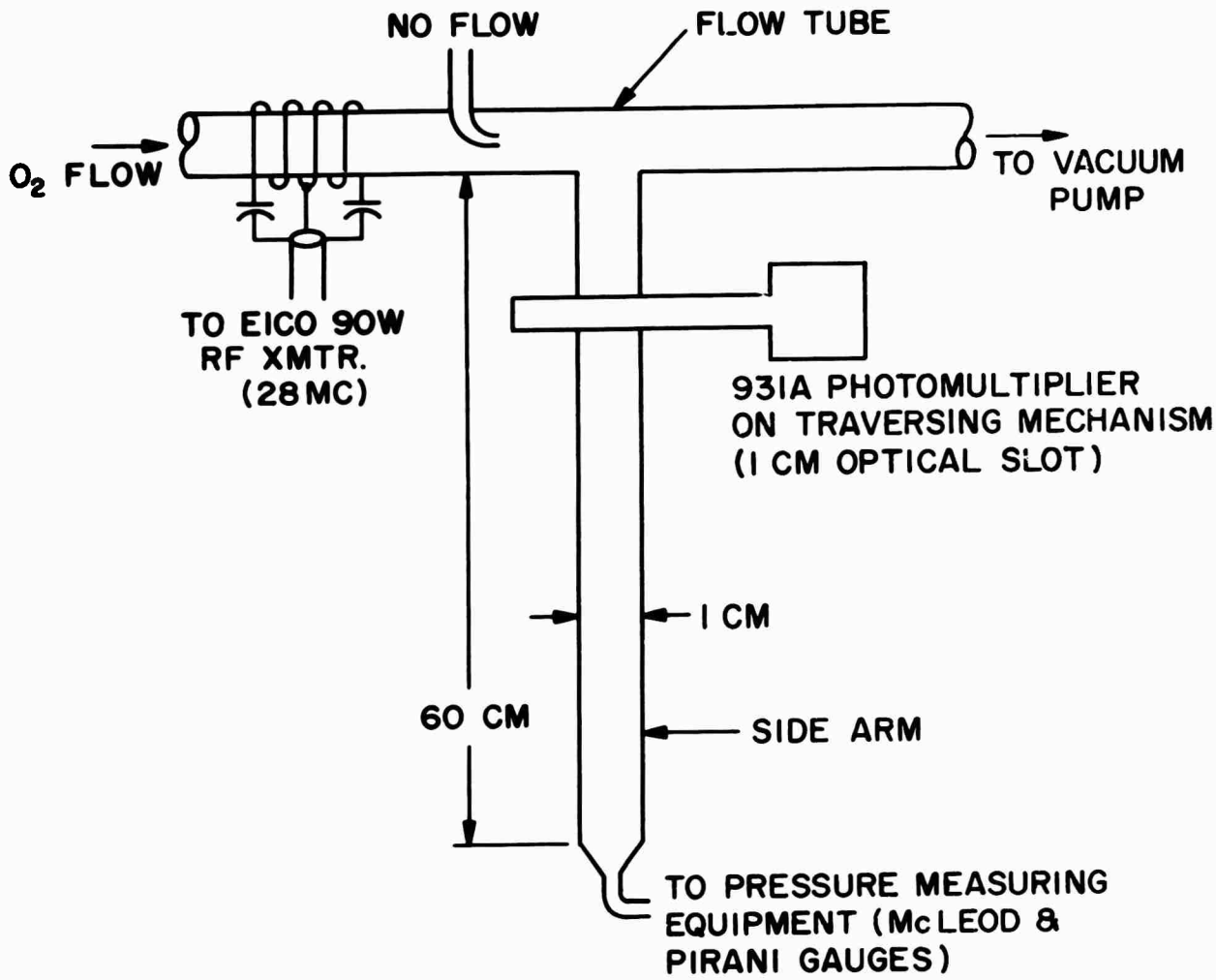

Fig. III-1 SCHEMATIC OF THE EXPERIMENTAL METHOD USED TO STUDY THE BEHAVIOR OF NO AS AN INDICATING CATALYST FOR O ATOMS

The entire photomultiplier housing was arranged to traverse the side arm for a distance of about 5-40 cm from the flow tube. The flow tube and side arm were constructed of pyrex glass of 1.2 and 1.0 cm dia., respectively, and no special precaution was taken to clean the glass surfaces. The output from the photomultiplier was attenuated and read on a recording potentiometer. The pressure was measured with a 0-10 mm McLeod gauge. These experiments were conducted in the steady state, and the object was to measure the decay of oxygen atom in the side arm and see how this decay was affected by the various physical parameters at our disposal (pressure, nitric oxide concentration, and oxygen atom concentration.)

A selection of the experimental measurements on the decay of the light intensity in the side arm is given in Figs. III-2, III-3, and III-4 where the effects of pressure, nitric oxide concentration, and oxygen atom concentration, respectively, are shown. For the data in Fig. III-3 the mole fraction of nitric oxide, X_{NO}, was computed assuming no O_2 dissociation (the degree of dissociation was small). Since no absolute O-atom concentration measurements were made, the effects of changing the relative values of O-atoms in the flow tube are given in Fig. III-4; a relative measure was provided by a monitor photomultiplier located on the flow tube at its junction with the side arm. By changing the loading on the transmitter and by detuning the gas-discharge tank circuit the O-atom concentration was varied by a factor of 25.

In the theoretical analysis we assume that the O-atom concentration is small so that density changes (through recombination) are unimportant, and that NO concentration is kept small to avoid the complications of multicomponent mixtures, i.e., O-atoms diffuse essentially through O_2. For constant temperature and pressure, the differential equation that governs the concentration of O-atoms,

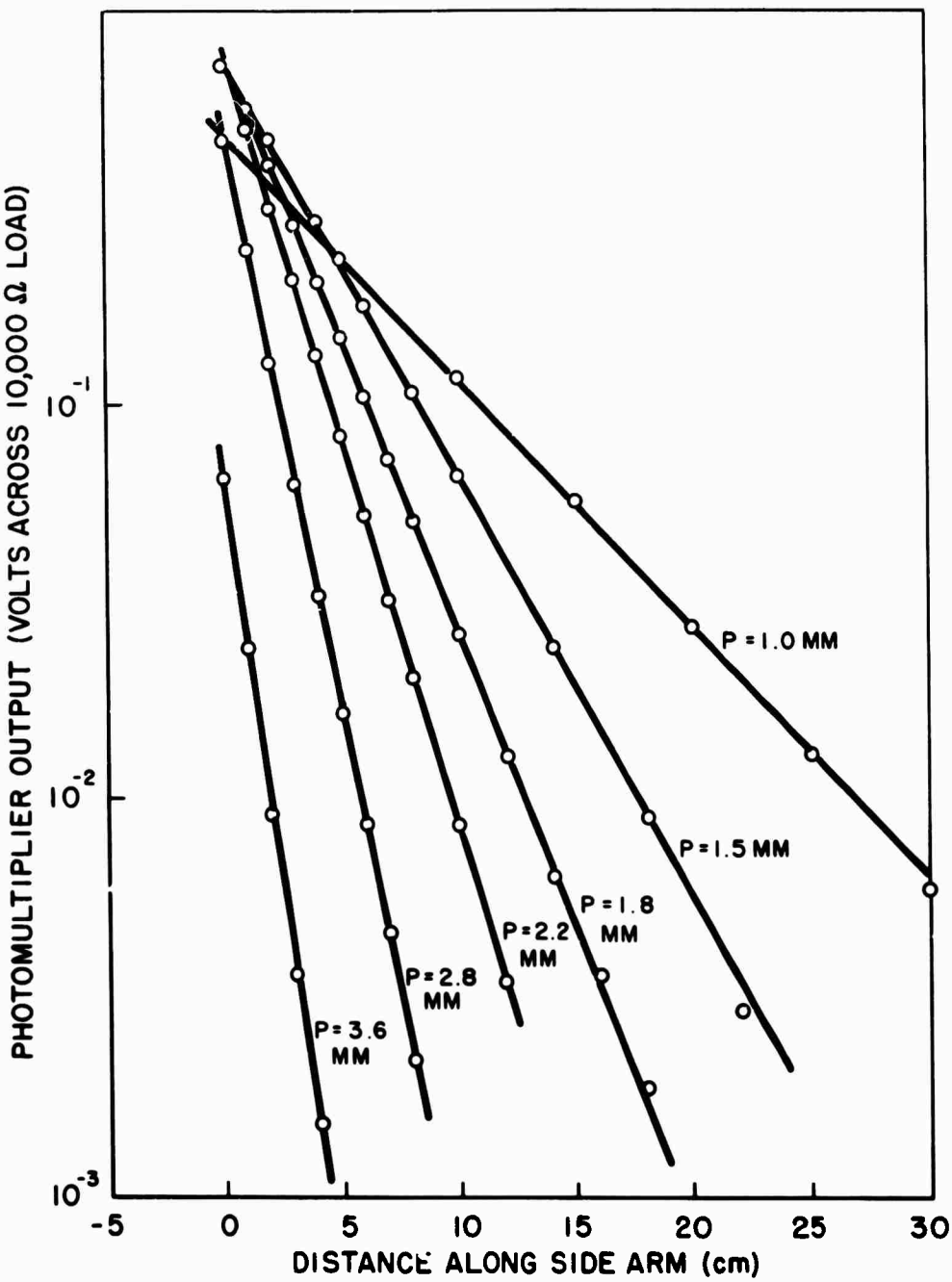

Fig. III-2 DECAY OF O ATOMS IN THE SIDE ARM AS INDICATED BY AIR AFTERGLOW EFFECT OF PRESSURE ($T = 300^{\circ}K$, $X_{NO} = 0.018$)

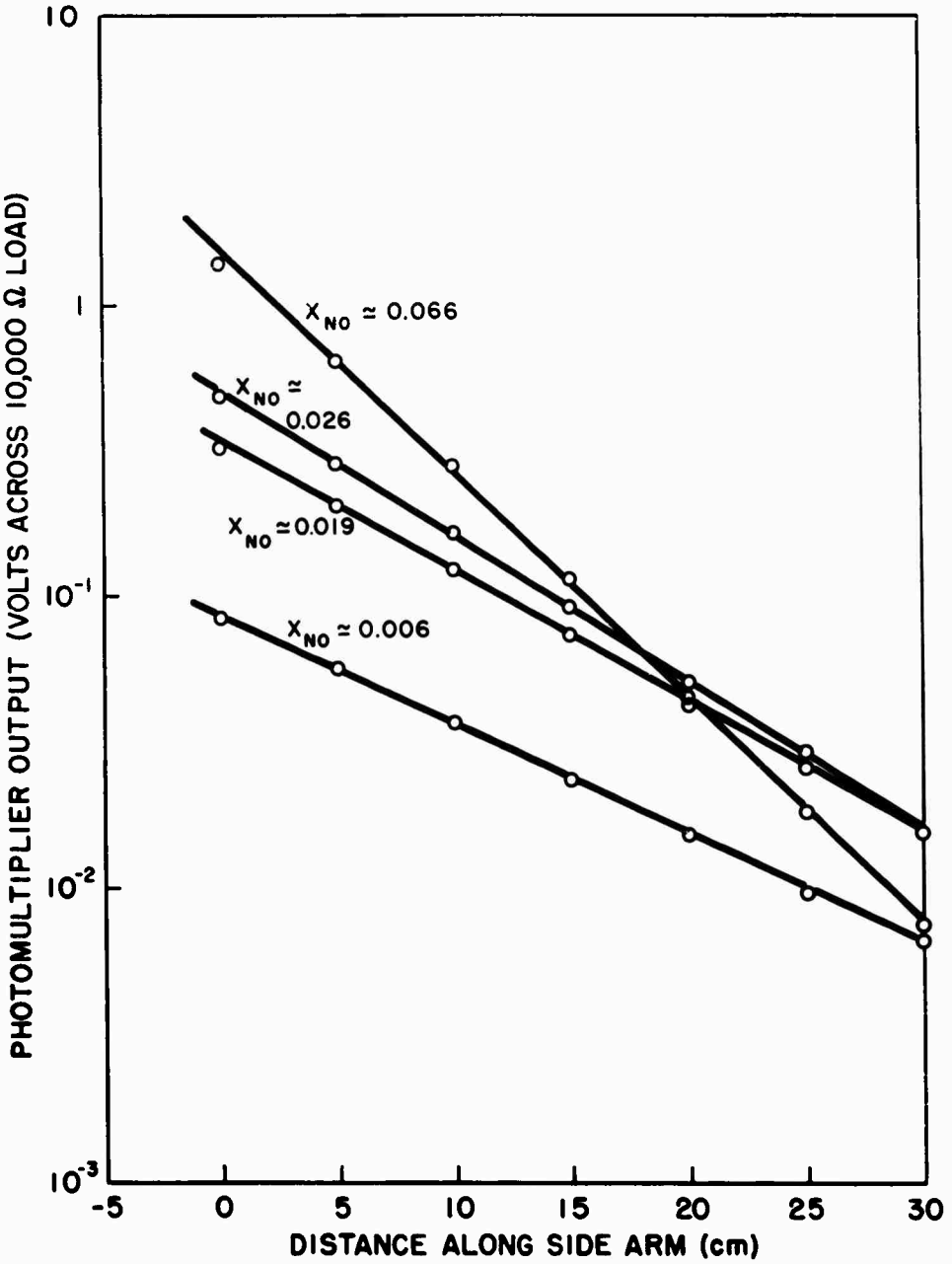

Fig. III-3 DECAY OF O ATOMS IN THE SIDE ARM AS INDICATED BY AIR AFTERGLOW - EFFECT OF NO CONCENTRATION (T = 300°K, P = 0.81 mm Hg.)

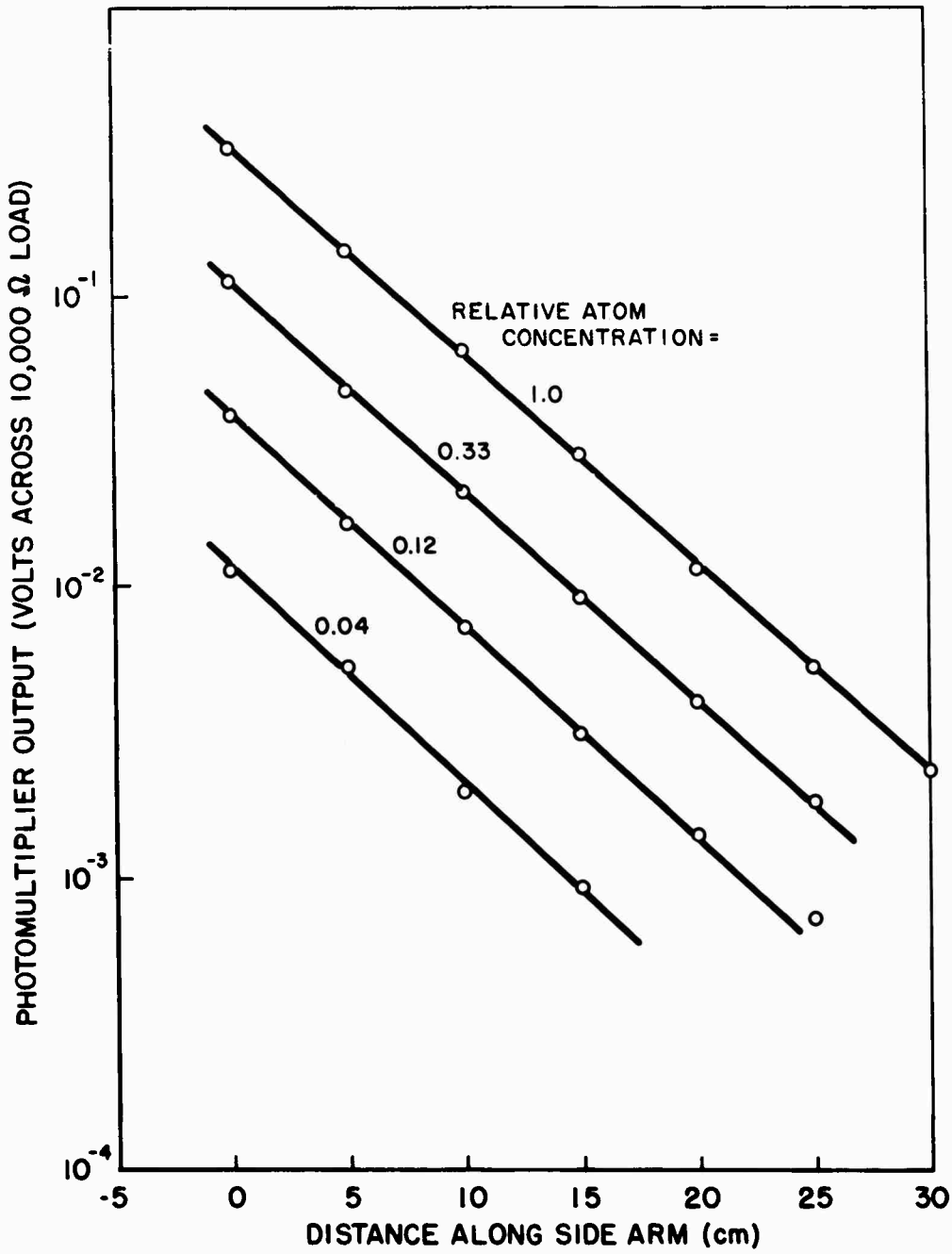

Fig. III-4 DECAY OF O ATOMS IN THE SIDE ARM AS INDICATED BY AIR AFTERGLOW EFFECT OF RELATIVE O-ATOM CONCENTRATION IN THE FLOW TUBE (T = 300°K, P = 0.97 mm Hg.)

$[O]$ is

$$D\frac{d^2[O]}{dz^2} = \frac{\gamma\bar{c}}{2R}[O] + 2\left\{k_1 + k_2[M]\right\}[NO][O] + k_3[M][O]^2 \qquad (4)$$

where the first term on the right is the loss of atoms through wall recombinations (no radial gradients are assumed to exist in the side arm), and the second verm is the removal of atoms through reactions (1) and (2) - the factor of two arising because of the rapid reaction (3). The final term on the right is the removal of atoms through three-body atom recombination

$$O + O + M \longrightarrow O_2 + M \qquad (5)$$

with a rate constant k_3. Because of the specific way in which reaction (5) affects the O-atom profiles in the side arm (see Ref. 1), the experimental data presented above indicate, for the conditions of the experiments, reaction (5) is not a significant reaction for O-atom removal and is not considered in the present analysis. Equation (4) then has a simple solution

$$[O] = [O]_o \exp(-\lambda z) \qquad (6)$$

where $$\lambda^2 = (\gamma\bar{c}/2RD) + 2\left\{k_1 + k_2[M]\right\}[NO]/D \qquad (7)$$

The nature of the solution given by Eq. (6) is in agreement with the data contained in Figs. III-2, III-3, and III-4. Additional proof of these arguments can be provided if one plots the slopes (λ) of the curves in Figs. III-2 and III-3 as a function of the appropriate varied parameter implied by Eq. (7). Figure III-5 is such a crossplot of λ^2 versus X_{NO} giving a straight line with a positive intercept established by wall recombination, $\lambda^2_{X_{NO}=0} = (\gamma\bar{c}/2RD)$,

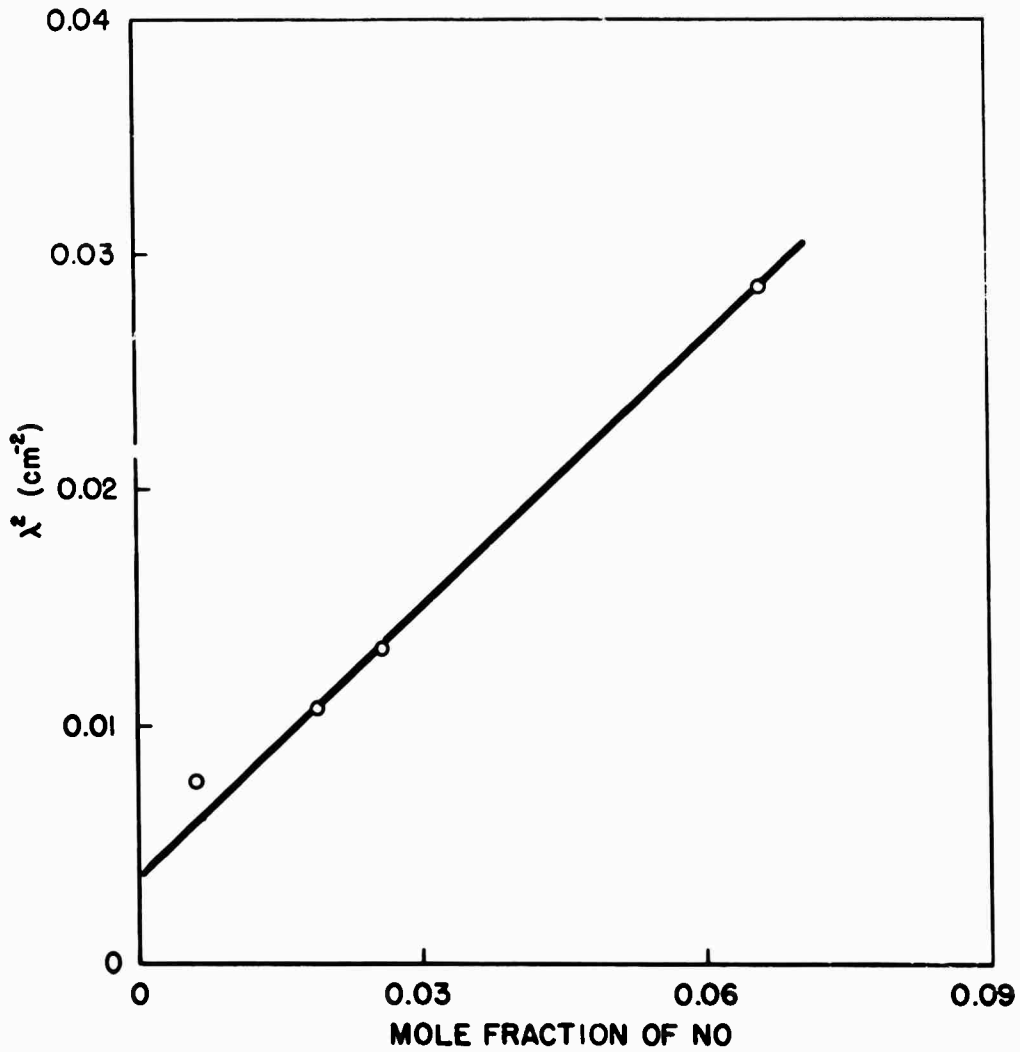

Fig. III-5 CROSSPLOT OF λ^2 VERSUS X_{NO} FOR THE DATA OF FIG. III-3

and a slope established by the kinetics of reactions (1) and (2), $\frac{d\lambda^2}{d[NO]} = 2\left\{k_1 + k_2[M]\right\}/D$. To analyze the data provided in Fig. III-1, we must use the pressure dependence of the diffusion coefficient, i.e., $D = D_o/P$, where D_o is the diffusion coefficient at one atmosphere and P is the pressure in atmospheres, and the fact that chemical species concentrations (mole cm^{-3}) as expressed in Eq. (7) are proportional to pressure. Figure III-6 is therefore a crossplot of λ^2 760/P versus P^2 (P in mm Hg). The existence of a straight line in this case indicates that reaction (2) is the most important mechanism for the loss of oxygen atoms. The slope of this line could be used to evaluate the rate constant k_2. Unfortunately, the diffusion coefficient must be known before catalytic activity, γ, can be evaluated from the intercepts of the curves in Figs. III-5 and III-6 and before the rate constant k_2 can be evaluated from the slopes of these curves. Using the average value of $D_{O-O_2} = 0.31$ cm^2/sec (P = 1 atm) reported by Krongelb and Strandberg, we have computed γ and k_2 for the data given in Figs. III-4 and III-5. The results are reported in Table 1 where comparison has been made with similar values reported in the literature. It is

Table 1. Values for the catalytic activity of a pyrex surface for oxygen atom recombination and for the rate constant of the reaction $O + NO + M \longrightarrow NO_2 + M$. ($T = 300^oK$)

Source	k_2 cm^6 $moles^{-2}$ sec^{-1}	γ
Fig. III-5	6×10^{16}	1.7×10^{-5}
Fig. III-6	4.3×10^{16}	0.4×10^{-5}
Kaufman (Ref. 3)	2.5×10^{16}	2×10^{-5}
Krongelb & Strandberg (Ref.1)		3.2×10^{-4} (quartz)
Linnett & Marsden (Ref. 4)		1.2×10^{-4}

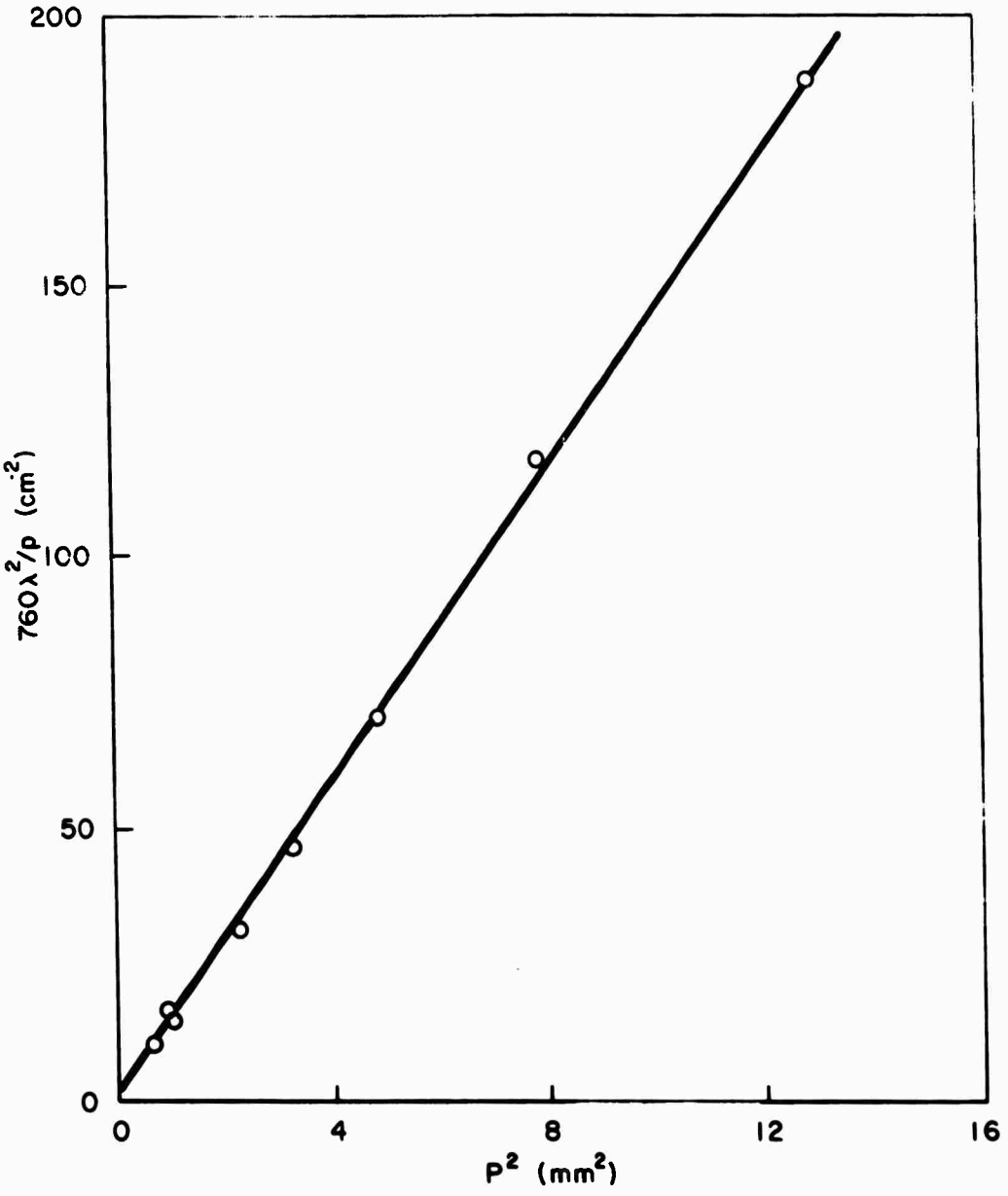

Fig. III-6 CROSSPLOT OF 760 λ^2/P VERSUS P^2 FOR THE DATA OF FIG. III-2

interesting to note that the catalytic activity of pyrex for O-atom recombination is consistently lower when NO is present (Ref. 3 and this work) than when special precautions are taken to purify the oxygen (Refs. 1 and 4).

Diffusion Coefficients using the Transient Method

The technique used by Krongelb and Strandberg (Ref. 1) to measure $D_{O\text{-}O_2}$ consists of measuring the transient decay of atoms at a particular position in the side arm after the source of atoms in the flow tube has been removed. For the ideal condition that the atom concentration in the flow tube falls immediately to zero at t = 0, the concentration of atoms at a particular position z and time t is given as

$$\left[O\right]_{z,t}\Big/\left[O\right]_{z,0} = 1 - \frac{1}{2}\,\mathrm{erfc}\left\{\left[\ /2(Dt)^{1/2}\right] - \lambda(Dt)^{1/2}\right\} + (e^{2\lambda z}/2)\,\mathrm{erfc}\left\{\left[z/2\ (Dt)^{1/2}\right] + \lambda(Dt)^{1/2}\right\} \qquad (8)$$

where λ is defined by the steady state Eq. (6). Equation (8) is difficult to fit to a general experimental transient curve; however, we have found that in terms of the half-time, $t_{1/2}$ where $\left[O\right]_{z,t_{1/2}} = 1/2\ \left[O\right]_{z,0}$, to a very good approximation

$$2\lambda z = 4\lambda^2 Dt_{1/2} - 1 \qquad (9)$$

Equation (9) permits a more rapid evaluation of a particular experimental curve. Furthermore, ambiguities arising from experimentally determining when t = 0 can be avoided by measuring transient atom concentration at two positions in the side arm a distance Δz apart. The time interval between the two respective half times $\Delta t_{1/2}$ can easily be used to determine D, since

$$D = \Delta z/2\lambda\Delta t_{1/2}\ . \qquad (10)$$

In our experiments two photomultipliers were placed approximately 10 cm apart on a carriage that could traverse the side arm. The outputs from the photomultipliers were fed directly to a two-channel Sanborn recorder having a chart speed of 10 cm/sec. In almost all cases studied the response of the recorder was sufficient to follow the transients. $t_{1/2}$ was of the order of 0.1 sec. Readability of the charts, in general, was no better than 5-10%. Although transient curves taken at a particular position along the side arm were reproducible, there is an inordinate degree of scatter between data taken at different positions along the side arm. Although several explanations for this scatter can be conceived, to date, the cause has not been reconciled. The data taken with this method are reported in Table 2. The average of all the values reported is D_o = 0.41 cm^2/sec with a probable error of about ±20%. This value is larger than the average reported by Krongelb and Strandberg, D_o = 0.31 cm^2/sec. It is hoped to eventually improve the precision of this technique.

Table 2. Diffusion coefficients for $O-O_2$ obtained with the transient method using NO as an O-atom indicator.

P (mm Hg)	λ (cm^{-1})	X_{NO} (approx.)	$t_{1/2}$ (sec)	D (cm^2/sec)	D_o (cm^2/sec)	Scatter (%)
.95	.151	0.016	0.098	335	0.418	7
1.31	.220	0.016	0.085	264	0.454	60
.97	.135	0.018	0.111	330	0.420	3
.95	.135	0.018	0.107	341	0.426	26
1.96	.251	0.018	0.127	154	0.396	19
.97	.087	0.011	0.145	392	0.500	11
1.57	.214	0.011	0.141	164	0.339	20
.97	.170	0.015	0.120	243	0.309	22
.97	.170	0.015	0.099	293	0.374	14

Diffusion Coefficients using the Counter-Flow Method

By imposing a mass flow through the side arm of the same chemical composition as the gases flowing through the flow tube, it is possible to alter the steady state oxygen atom concentration in the side arm in such a manner that the diffusion coefficient can be conveniently isolated and measured. If the flow is assumed one-dimensional with a uniform* velocity U, Eq. (4) must be altered to include the convective term and becomes

$$D \frac{d^2[O]}{dz^2} - U \frac{d[O]}{dz} = \frac{\gamma \bar{c}}{2R} [O] + 2\left\{ k_1 + k_2 [M] \right\} [NO][O] \qquad (11)$$

where the three-body oxygen-atom recombination has been neglected. The solution of Eq. (11) is of the same form as Eq. (6) where

$$\lambda = (U + \sqrt{U^2 + 4D^2 \alpha^2}) / 2D \, . \qquad (12)$$

The parameter α is the value for λ when the stream velocity is zero. Since the stream velocity will normally be computed from a known quantity of gas flow measured for NTP conditions ($\dot{V}$ cm^3/sec at NTP) and since $D = D_o/P$, the diffusion coefficient reduced to one atmosphere, D_o, can conveniently be computed from a rearranged form of Eq. (12)

$$D_o = \dot{V} \lambda / A (\lambda^2 - \alpha^2) \qquad (13)$$

where A is the cross-sectional area of the side arm. For this reason, the possible inaccuracy due to vacuum pressure measurements can conveniently be avoided. (If the temperature of the side arm is other than room temperature, appropriate temperature corrections must be included.) If necessary, the parameter α can be eliminated by using two general curves with counterflow

* The complications of Poiseuille flow are presently being investigated.

$$D_o = (\lambda_1 \dot{V}_1 - \lambda_2 \dot{V}_2)/A\,(\lambda_1^2 - \lambda_2^2)\,. \qquad (14)$$

Because the values for $\dot{V}$ are quite small and because the same chemical composition is required in both the flow tube and side arm flow, the O_2 and NO were premixed and then metered to the respective tubes. This procedure, although expedient at the time, may have introduced some ambiguities because of the equilibrium formation of NO_2 before the gas mixture is used in the experiment. Some preliminary data obtained in this way are presented in Fig. III-7, where it is seen that the data are in qualitative agreement with the theory. Average diffusion coefficients determined from three such sets of experimental data are D_o = 0.31, 0.29, and 0.35 cm^2/sec. These are in good agreement with the values reported by Krongelb and Strandberg. Although several experimental difficulties with this technique have been encountered, the results have been quite encouraging. Because of the decided advantages of this method over the transient method, it will be explored in more detail.

References

1. S. Krongelb and M. W. P. Strandberg, J. Chem. Phys. 31, 1196 (1959).
2. Task R Quarterly Progress Report No. 3, 1 October - 31 December 1959. The Johns Hopkins University, Applied Physics Laboratory Report No. TG-331-3 (January 1960).
3. F. Kaufman, Proc. Roy. Soc. A247, 123 (1958).
4. J. W. Linnett and D. G. H. Marsden, Proc. Roy. Soc. A234, 489 (1956).

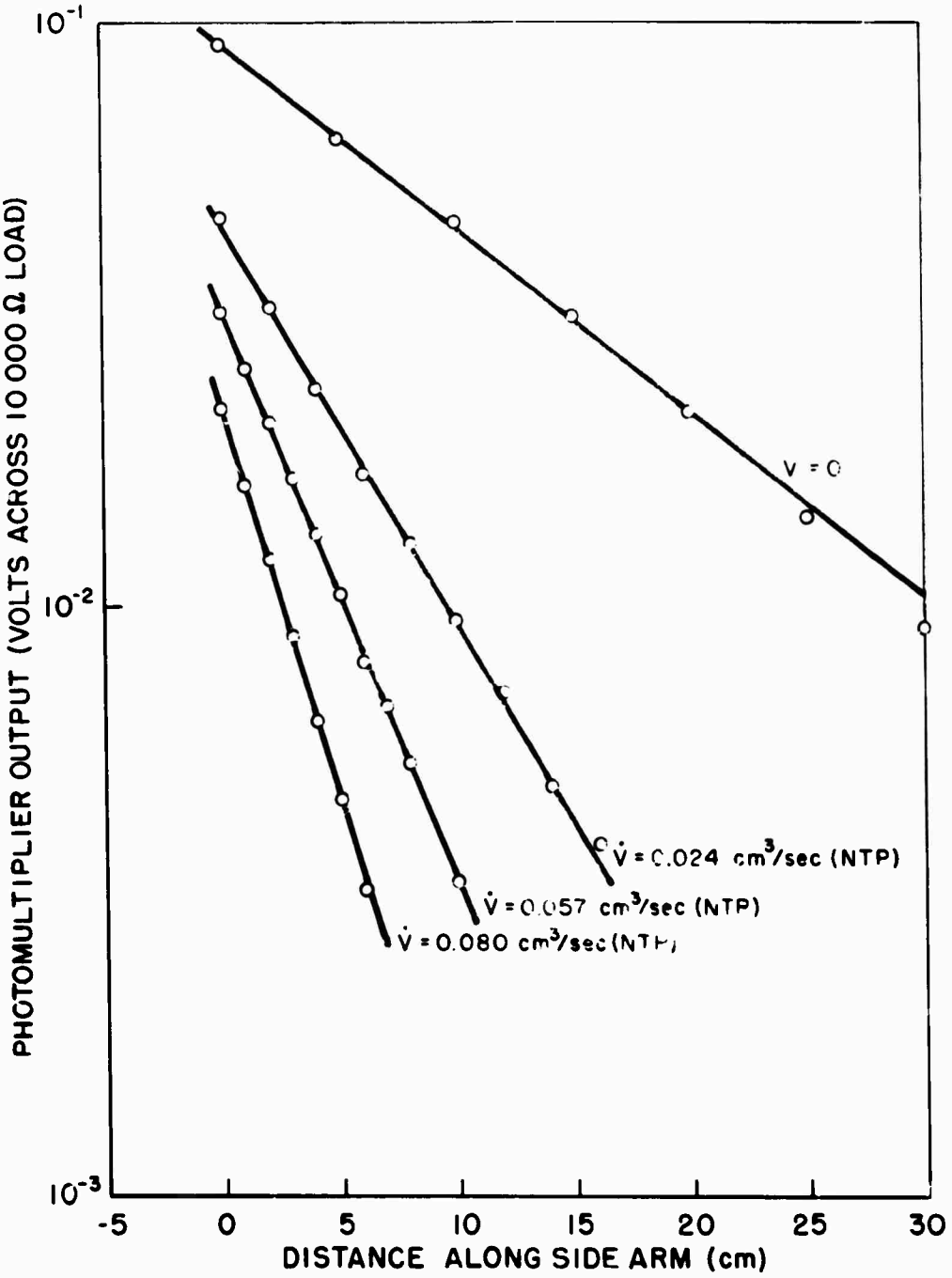

Fig. III-7 DECAY OF O ATOMS IN THE SIDE ARM AS INDICATED BY AIR AFTERGLOW EFFECT OF CROSSFLOW IN THE SIDE ARM (T = 300°K, P = 0.43 mm Hg.)

IV. HIGH TEMPERATURE CHEMICAL KINETICS FROM A REACTING POINT SOURCE

(M. L. Snow and A. A. Westenberg)

Objective

One of the difficulties in the way of adequate understanding of the aerodynamics of high temperature, high speed gas flow has been the lack of information about the chemical kinetics involved. Obtaining this information has been difficult, especially in those cases where premixing the reactants before bringing them to reaction temperature is impossible because of the rapidity with which the reaction proceeds. Laminar flame studies such as are discussed in Section I, are one way of acquiring high temperature kinetic data if the reactants can be premixed. Another approach is to adapt and utilize the point source technique (Ref. 1) used for the measurement of diffusion coefficients, a method which should be especially useful when premixing is impossible. This technique will allow preheating of the reactants before mixing, steady-state operation, a fair temperature range, and simple pseudo-first order kinetics for analysis. Thus it can be seen that information obtained by this method might be a useful supplement to that obtained in the laminar flame work.

Theory of the Method

The theory has been described in some detail in Ref. 2.

Experimental

Exploratory work with the $CO-O_2$ system has been temporarily laid aside. Although the scheme for detection and analysis as described in Ref. 2 works quite well, an onerous problem with the injection system remains. Unfortunately, in the temperature range of interest ($\sim 1000^{\circ}K$), carbon monoxide is strongly disposed

to undergo the disproportionation reaction $2CO \rightarrow CO_2 + C$, especially on a metal surface. The carbon formed in this process quickly plugs up the injection tube, making further experimentation difficult.

It has been suggested that, inasmuch as the reaction is catalyzed by the metal surface of the tube, this carbon formation could be prevented by first poisoning the surface with hydrogen sulfide, a known catalyst poison. (Presumably a film of FeS would be formed on the steel tube.) An attempt will be made in this direction as soon as the approach described below has been studied.

As an alternate to the $CO-O_2$ reaction, it was decided to use the H_2-O_2 reaction to test the feasibility of the method. This necessitated a minor change in the analysis scheme. The procedure is to analyze for the residual hydrogen remaining in the gas mixture. To do this, the sample drawn into the probe is passed through a liquid nitrogen trap to remove all water and then goes directly to the sample side of the thermal conductivity cell. From there, it is passed over a heated platinum catalyst to oxidize the hydrogen to water which is removed in a second liquid nitrogen trap. The resulting pure oxygen (or air), the reference gas, then flows into the other side of the T-C cell.

Results

Some preliminary results have been obtained by this method and will be described below. Initial attempts to use H_2 injected into pure O_2 were unsuccessful at the temperature used ($\sim 1000^{\circ}K$) because the reaction was too rapid. All the H_2 reacted upstream of the closest practical sampling position. It was then decided to use air as the carrier gas to slow down the reaction.

The data obtained in the first of two successful runs with air are presented in Fig. IV-1. The concentrations are given in millivolts since

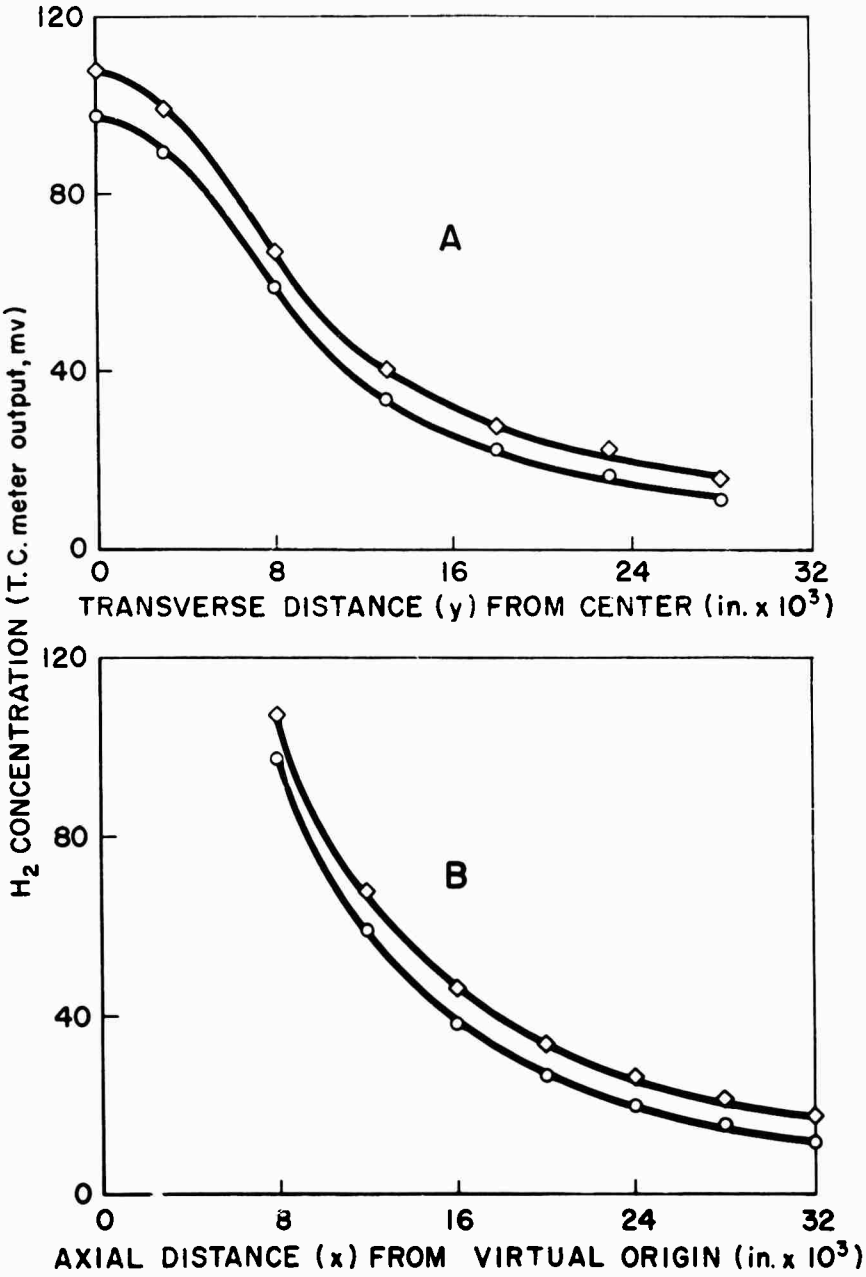

Fig. IV-1 H_2 CONCENTRATION DOWNSTREAM OF POINT SOURCE IN AIR CARRIER
T = 1030°K, P = 1 atm. O: Experimental data with reaction occurring. ◊: Hypothetical distribution with no reaction. (A) Transverse distribution at x 0.008 in. (B) Axial distribution at y = 0.

the output of the T-C cell is a linear function of the H_2(trace) concentration. The axial distance has been corrected for the virtual origin effect (described in Ref. 1). From Eq. (3) of Ref. 2, it can be shown that, for axial decay the quantity log (c • x) should be a linear function of x. By successive approximations, a correction to the measured x is found so that the above condition is satisfied, which establishes the virtual origin.

As discussed in Ref. 2, the axial decay data are to be plotted as log $(c_2\ x_2/c_1\ x_1)$ vs. $(x_2 - x_1)$ having slope m_1 related to the pseudo-first order rate constant by

$$k = D\ m_1^2 - U\ m_1 \qquad (1)$$

(Eq. (4) of Ref. 2 contains an error. It should read as above.) Such a plot for the data of Fig. IV-1B is shown in Fig. IV-2, where various pairs of data at different axial distances x were used. The line represents a least squares fit of the data. The points show relatively little scatter when one realizes that if there were no reaction this line would be coincident with the abscissa, i.e., cx would be constant. Yet, as can be seen from Fig. IV-1B, the Concentration-Distance plot for the case where no reaction occurs* is but little different from that in which it does.

The transverse profile data such as are given in Fig. IV-1A were similarly plotted as log $(c_2\ r_2/c_1\ r_1)$ vs. $(r_1 - r_2)$ with slope m_2 related to k by

$$k = D\ m_2^2 - U^2/4D. \qquad (2)$$

---

* The no-reaction curves of Fig. IV-1 may be shown to be related to those with reaction by

$$\ln \frac{c\ (\text{no reaction})}{c\ (\text{reaction})} = -\ m_1 x\ (\text{axial}) = -\ m_1 r\ (\text{transverse})$$

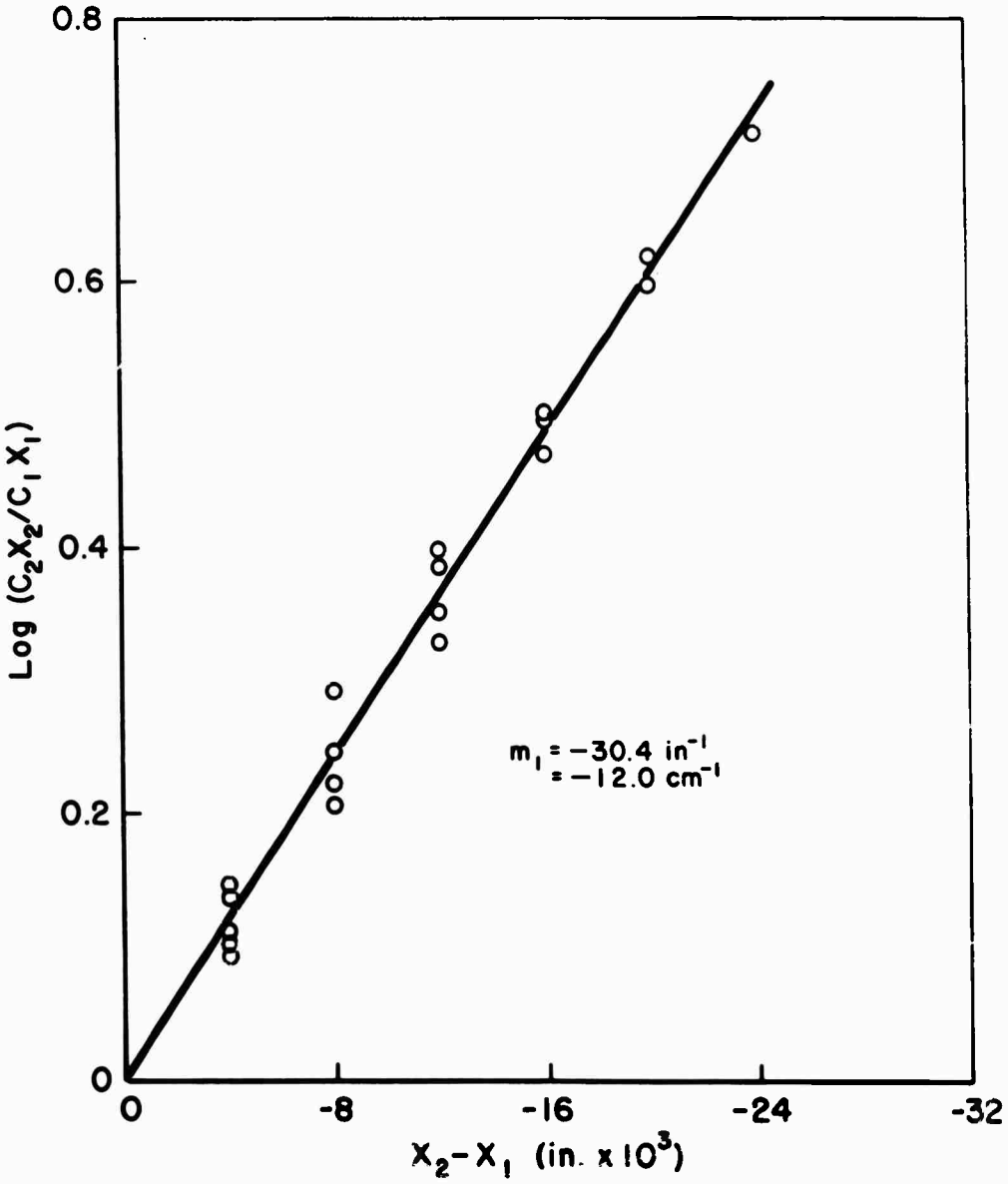

Fig. IV-2 LOG (c_2x_2/c_1x_1) VERSUS DIFFERENTIAL AXIAL DISTANCE FOR DATA OF FIG. IV-1B
Points represent results using various pairs of data.

From Eqs. (1) and (2)

$$k = - D m_1 (m_1 + 2m_2) . \qquad (3)$$

The results obtained from two runs are summarized below in Table I.

Table I

Run #	T(°K)	$D_{H_2-O_2}$	$m_1(cm^{-1})$	$m_2(cm^{-1})$	$k(sec^{-1})$
1	1030	7.29	- 12.0	15.5	1660
2	1020	7.17	- 10.6	28.7	3560

Discussion

It may be noted that the two values of k given in Table I differ by more than a factor of 2. Whether this is the type of precision to be expected remains to be seen. It is felt that the difference might be traced to the fact that Run #1 was made using laboratory air for the carrier gas whereas Run #2 was made using bottled compressed air. The latter, having fewer contaminants, could well lead to a faster reaction rate. This will be checked. At any rate, it now appears that this method shows some promise for determining over-all reaction rates. It has the necessary sensitivity and, if the reproducibility proves to be good, the method may be a handy tool in the study of the kinetics of gas reactions.

References

1. R. E. Walker and A. A. Westenberg, J. Chem. Phys. 29, 1139 (1958).

2. M. L. Snow and A. A. Westenberg, Task R Quarterly Progress Report No. 3 for the period 1 October - 31 December 1959. The Johns Hopkins University, Applied Physics Laboratory Report No. 331-3 (January 1960).

V. ROCKET NOZZLE FLUID DYNAMICS

(F. K. Hill, H. J. Unger, S. A. Elder, and H. A. Wallskog)

Objective

The investigations carried out in this problem are concerned with the dynamics of the high speed gas flows occurring in solid propellant rocket nozzles. With high temperatures and large mass flow rates and with rapid expansion of the gas through the nozzle, it is important to describe the fluid properties taking into account non-equilibrium and non-ideal gas conditions. Experimental data pertinent to an accurate description of the gas are the first objective so that an adequate theory of the fluid dynamic behavior may be formulated.

In order to provide realistic and representative testing conditions for the experiment a double-base solid propellant (ARP)* has been chosen which provides the five basic constituents common to most high impulse propellants. These are hydrogen, nitrogen, carbon monoxide, carbon dioxide and water vapor. Impurities of the order of 2 to 3% are present as is the case in all propellants and it is possible to add in well controlled amounts and sizes solid particles for future extensions of the experimental studies. To begin with, it is believed advisable to keep the problems as uncomplicated as possible while still retaining the fundamental aspects of the phenomena under investigation. Combustion pressure and temperature of the grain are 1000 psi, nominal and 2500°K, respectively; end burning is employed for either 10-second or 30-second operation. These conditions are sufficient to introduce measurable effects due to the variable gas properties as the gas expands through the nozzle, gas non-equilibrium

---

* The propellant is manufactured and proof-tested at Allegany Ballistics Laboratory.

conditions in the expanded flow and heat transfer and nozzle divergence angle effects. Associated phenomena, such as erosion and deposition of solid particles, are also present for observations providing additional data.

It is anticipated that as the work progresses higher specific impulse propellants will be utilized providing temperatures in the 3000°K to 4000°K range, and that investigations of the effects of metal additives to the grain will be carried out. Cooling and heat transfer measurements to the nozzle walls will be made and some properties of materials directly associated with the rocket gases may be undertaken.

Introduction

The measurement of flow characteristics, gas properties and thermal levels has been continued using the propellant and experimental apparatus described heretofore. The present series of tests were intended to provide an accurate determination of the flow field in the region of low expansion ratio, as well as useful developmental tests for instrumentation relative to temperature and gas composition measurements. The results of these experiments were compared with theoretical predictions of nozzle performance and the effects of gas non-equilibrium behavior evaluated. As a logical extension of the present experimental program, future tests will involve more energetic propellants with their corresponding higher combustion temperatures.

Nozzle Surveys

The previous Quarterly Progress Reports (Refs. 1, 2, 3) contain a description of the equipment involved in the flow surveys of the 26° and the 12.5° nozzles. In this series of tests two or three fixed pitot probes were installed in the nozzles at the station where the expansion ratio is 5.85. This station was surveyed in

detail by locating the probes at appropriate cross-stream positions from test to test. During this period, two additional tests were conducted using the 12.5° nozzle in order to define the pitot pressure profile better, particularly in the region near the center line. The data obtained in the 12.5° total divergence angle nozzle are summarized in Fig. V-1 and compared to the profile expected for pure radial flow. The computed profile is based on one-dimensional flow with the assumption that the flow is in chemical equilibrium until the static temperature reaches 1500°K and is frozen thereafter, and includes an estimate of the boundary layer displacement thickness.

It appears, therefore, that the lengthening of the nozzle provides sufficient transit time for the gas to achieve chemical equilibrium while the data from the 26° nozzle, illustrated in the previous report (Ref. 3), showed a departure from simple conical flow. This measured deviation from assumed behavior may be due to chemical non-equilibrium effects; additional tests at different values of expansion ratio will determine if this can be attributed to chemical effects or is simply the result of flow distortion in the larger divergence angle case.

Gas Composition Observations

1. Infrared Spectrometer

The study of the determination of the gas composition of the combustion products from the high-temperature rocket tunnel during flow by infrared (I.R.) absorption techniques was continued during this report period with considerable success. Tests 71 and 72, previously reported in Ref. 3, indicated that the technique of using a cross-section of the tunnel as an I.R. absorption cell was feasible if the cell windows were flushed with dry nitrogen during the run

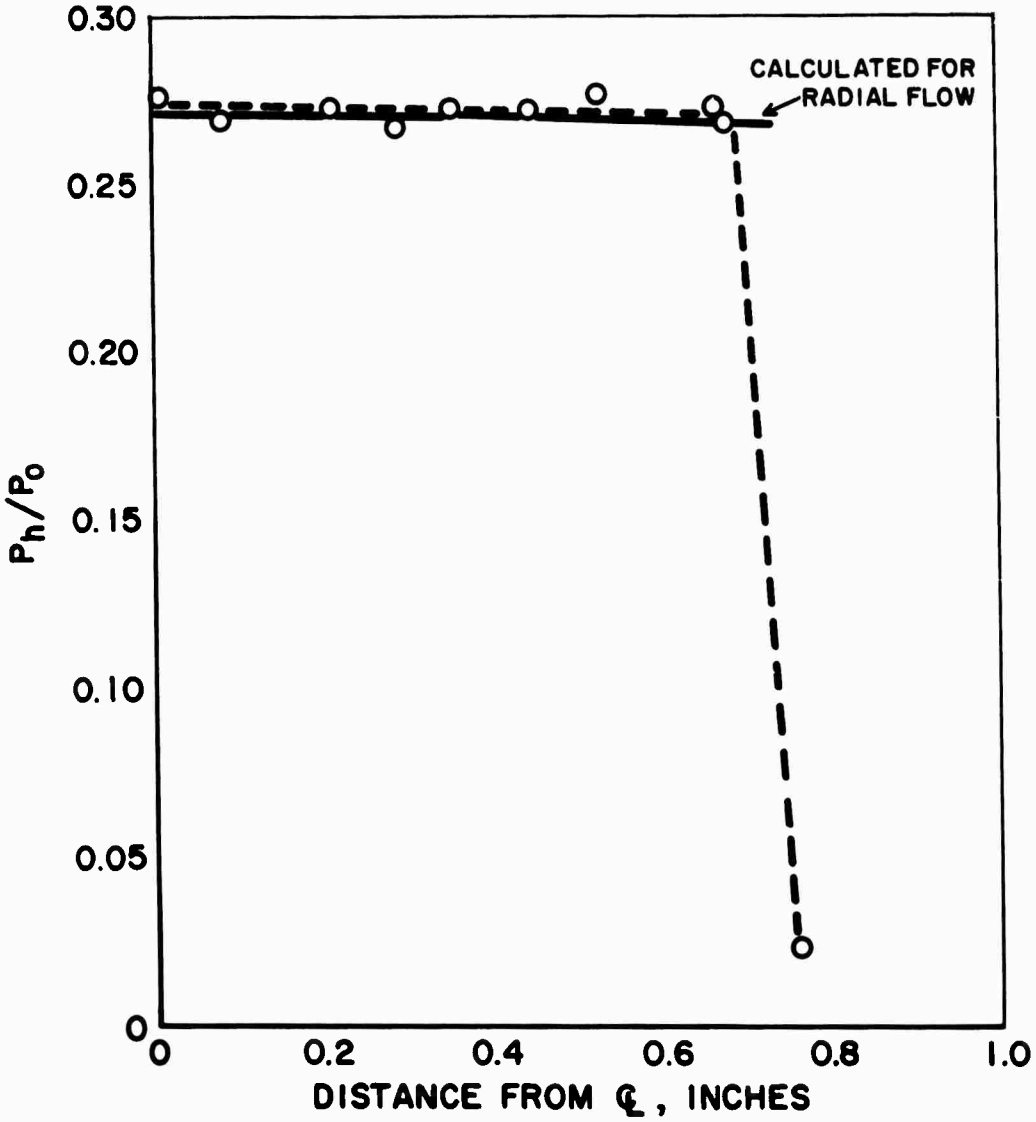

Fig. V-1 PITOT PRESSURE (P_h/P_o) DISTRIBUTION FOR THE 12.5° TOTAL EXPANSION ANGLE NOZZLE

to prevent fogging. Originally, quartz windows were used, but the technique has been demonstrated to be applicable for such a fragile material as rock salt. For this reason, it is felt that almost any I.R. transmitting material could be used for cell windows when properly mounted and flushed with a dry inert gas. At present, sapphire windows are in use and have gone through many tests without harm to the optical surfaces.

The above-mentioned tests showed that microphonics still was a problem in the detector system, which consisted of a PbSe photoconducting cell at ambient temperature feeding into a subminiature triode cathode follower. Potting the detector and cathode follower circuit in "Silastic" helped, but did not completely solve the microphonics problem. Since the dark resistance of the detector was about 100 K ohms, a transistor stage with a common collector was substituted for the triode stage. This proved to be sufficiently non-microphonic without potting to warrant a complete test with no other objective than to prove the reliability of the new optical bench system.

The source and collimating mirror system were enclosed in a brass box to allow flushing with dry air or nitrogen. This permitted the entire light path to be purged of water vapor and CO_2 except for the cell. Fig. V-2 is a reproduction of the CRO display of the response of the detector system to radiation from a Nernst glower with the entire optical path flushed with super-dry nitrogen. Fig. V-19(upper) is a similar display without flushing showing the H_2O and CO_2 absorption bands in the atmosphere from 1-3.5μ. It is evident that there is a small amount of absorption at 2.7μ due to both H_2O and CO_2, but it would require a vacuum system to remove this.

The following figures are reproductions of pictures taken of the CRO display of the rapid scan spectrometer detector output. The scanning rate was 60 cps giving a scanning time of less than 1/120 sec. In Test 84 the source was a Nernst glower running at 0.75 amperes. In Test 85 the source was a molybdenum probe heated by the gas flow. Moving pictures were taken of the CRO screen at 24 frames per second.

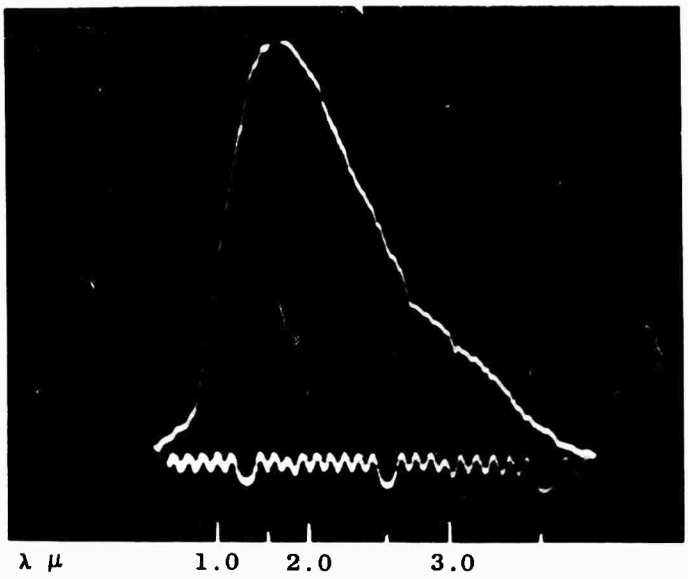

Fig. V-2 FIRST FRAME BEFORE IGNITION OF PROPELLANT IN TEST 84.

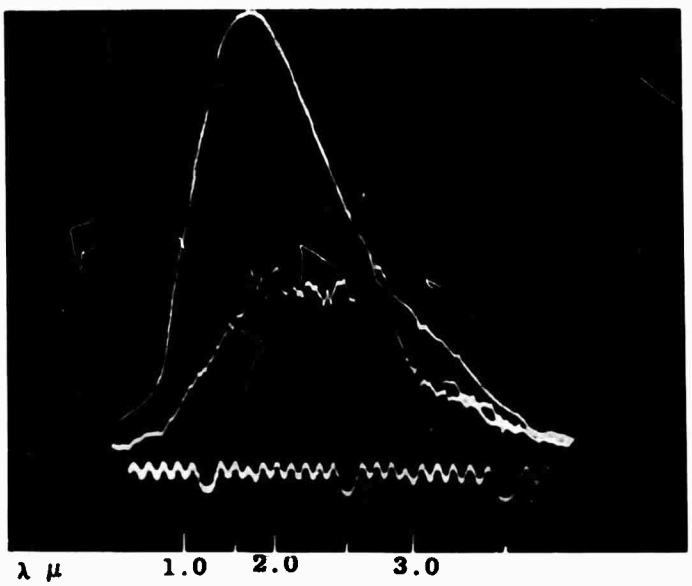

Fig. V-3 TEST 84. SPECTROMETER RESPONSE AT TIME OF IGNITION OF THE BLACK POWDER PRIMER. Fig. 2 IS SUPERIMPOSED TO SHOW CO_2 EMISSION BAND AT 2.7μ.

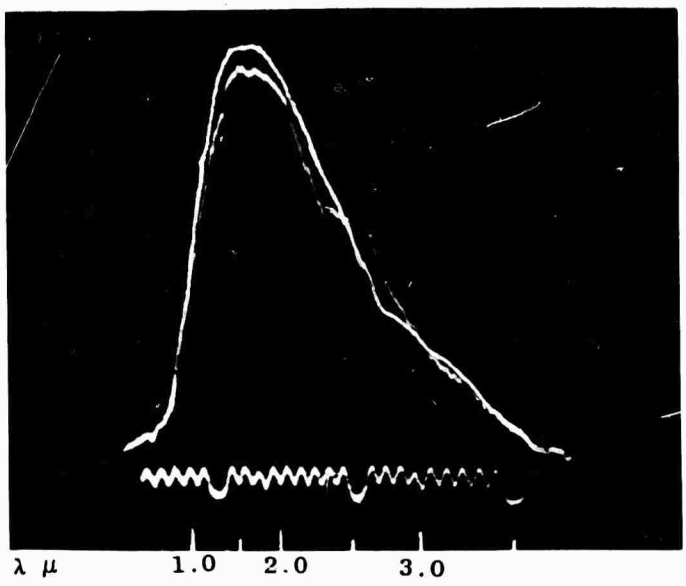

Fig. V-4 TEST 84. THE SECOND FRAME AFTER IGNITION SHOWING ALMOST COMPLETE RECOVERY OF TRANSMISSION THROUGH THE CELL WITH SOME ABSORPTION AND EMISSION STILL EVIDENT. Fig. 2 SUPERIMPOSED FOR REFERENCE.

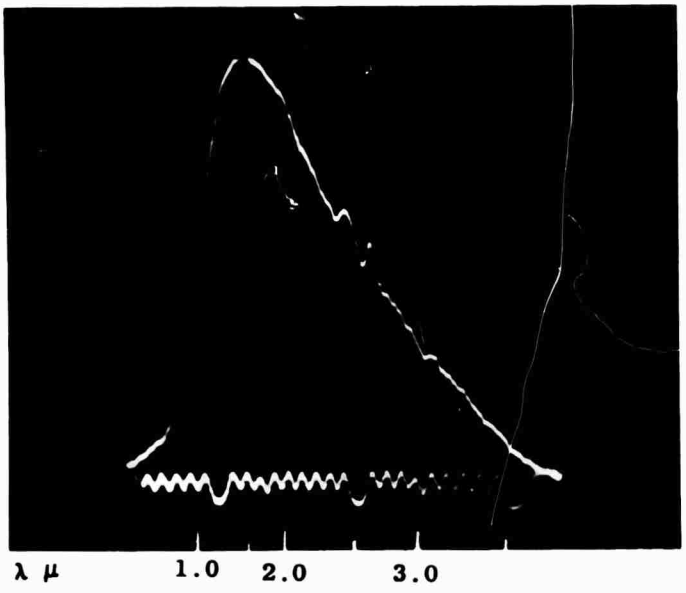

Fig. V-5 TEST 84. THE THIRD FRAME AFTER IGNITION.

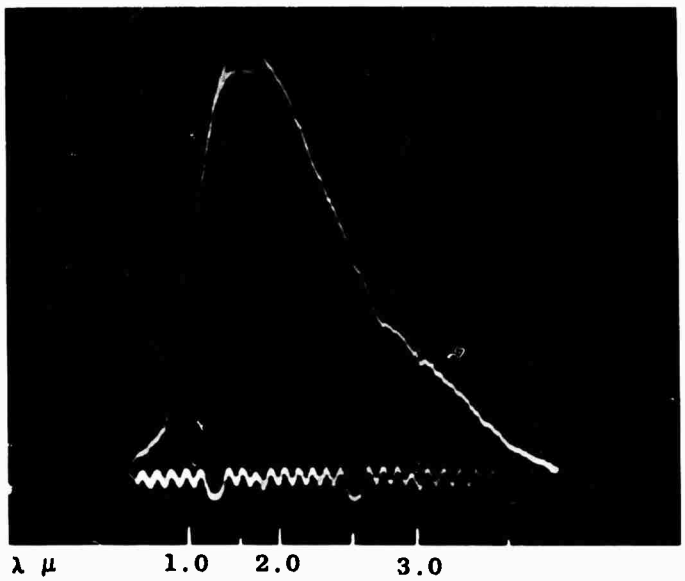

Fig. V-6 TEST 84. THE SIXTH FRAME AFTER IGNITION (0.25 sec.) COMPLETE RECOVERY OF THE EMISSION CURVE IS SHOWN. (SEE Fig. 2).

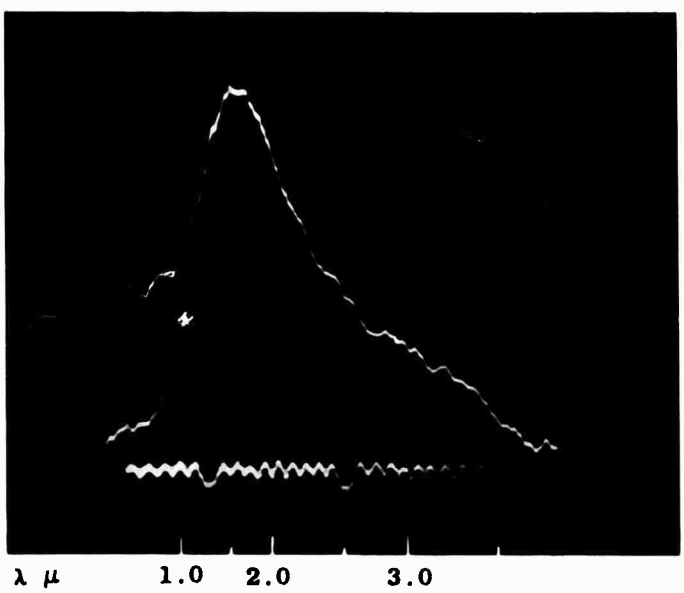

Fig. V-7 TEST 84. TWO SECONDS AFTER IGNITION.

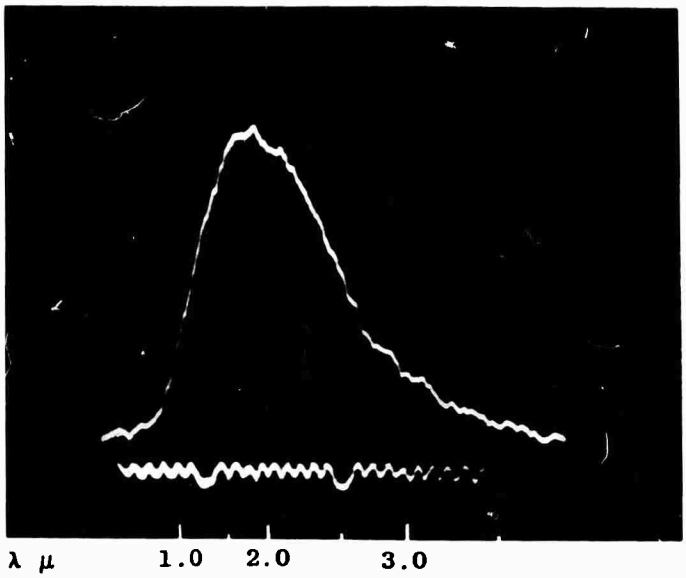

Fig. V-8 TEST 84. SIX SECONDS AFTER IGNITION.

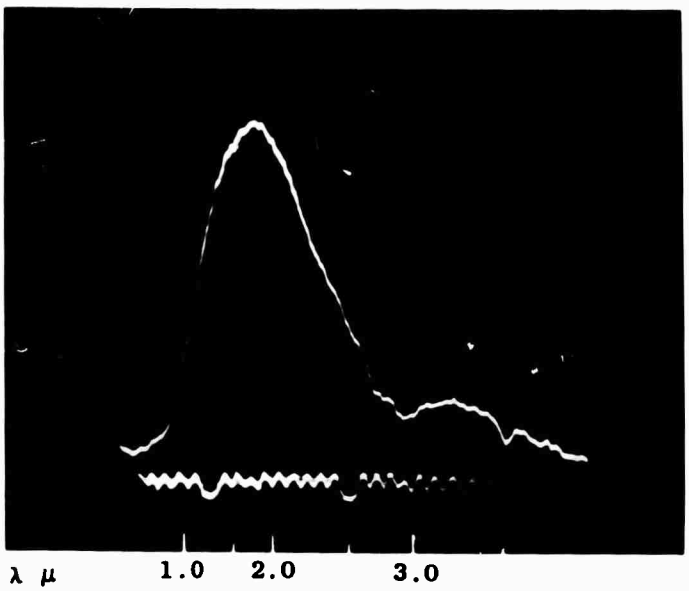

Fig. V-9 TEST 84. EIGHT SECONDS AFTER IGNITION.

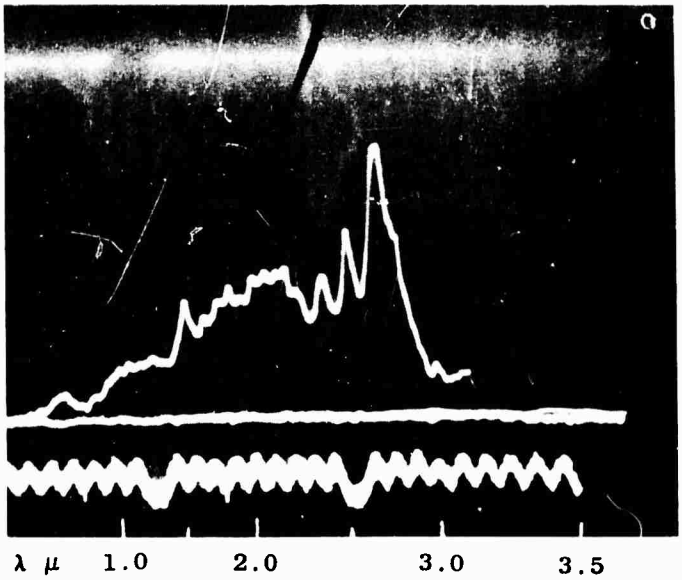

Fig. V-10 TEST 85. EMISSION CURVE FROM THE BLACK POWDER IGNITER. CO_2 AND H_2O EMISSION BANDS.

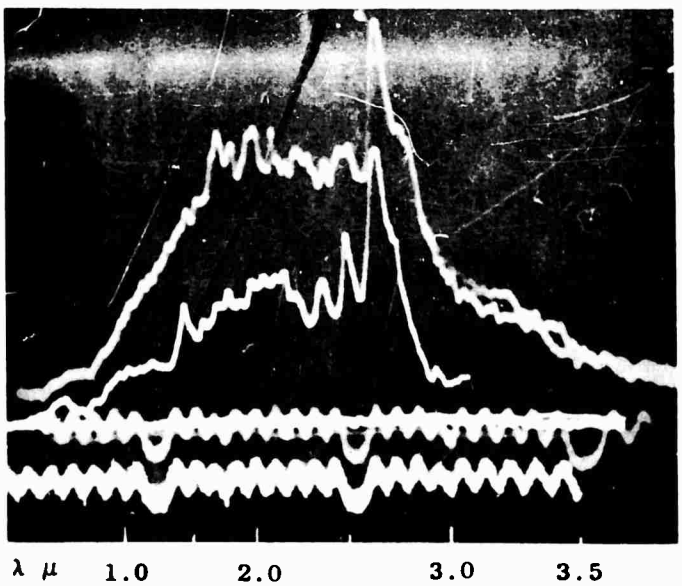

Fig. V-11 TEST 85. Figs. 3 (TEST 84) AND 10 SUPERIMPOSED FOR PURPOSE OF COMPARISON.

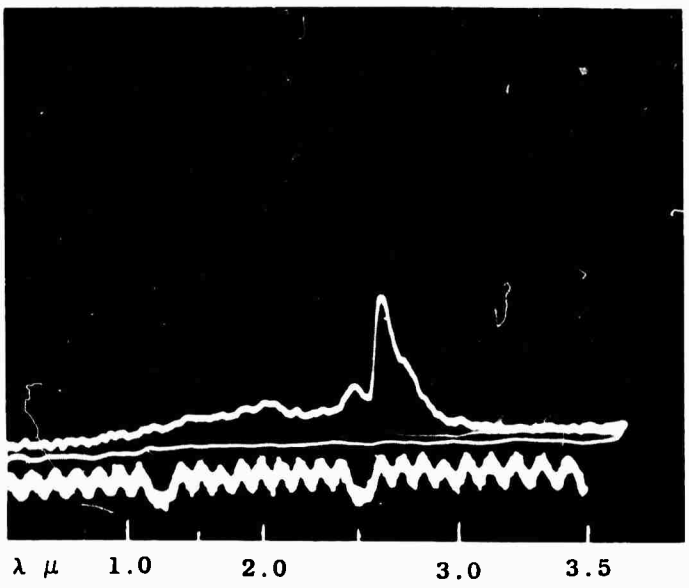

Fig. V-12 TEST 85. THE SECOND FRAME AFTER IGNITION SHOWING ONLY THE CO_2 AND H_2O EMISSION BANDS AT 2.7μ.

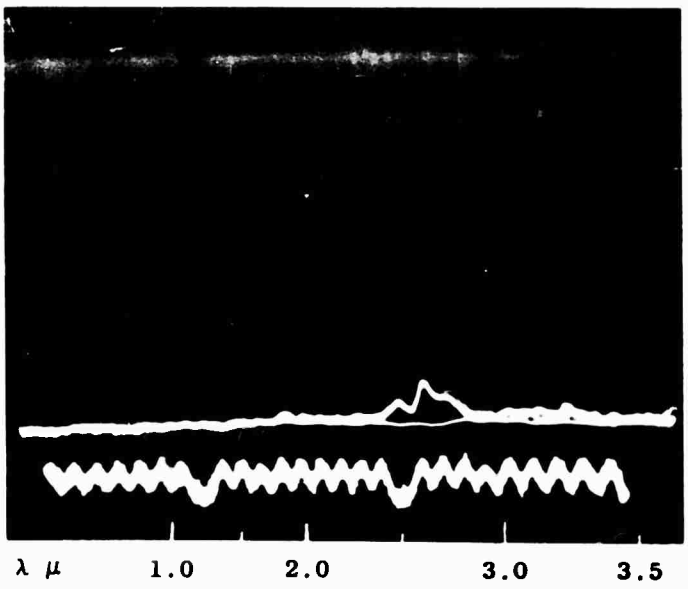

Fig. V-13 TEST 85. THE THIRD FRAME AFTER IGNITION. THE EMISSION FROM THE EXPLOSION IS NEARLY GONE WHILE THE PROBE HASN'T BEGUN TO RADIATE.

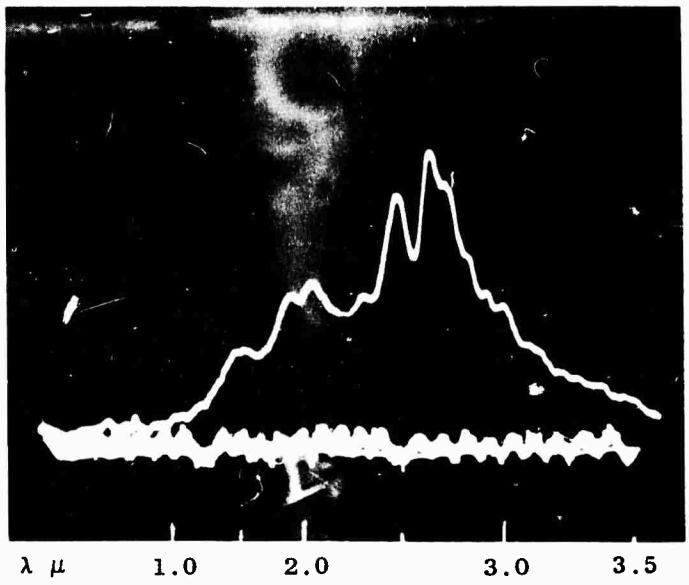

Fig. V-14 TEST 85. THE EMISSION CURVE 2.5 SEC. AFTER IGNITION. THE TEMPERATURE OF THE PROBE IS RISING AND THE CO_2 AND H_2O EMISSION BANDS ARE STILL PROMINENT.

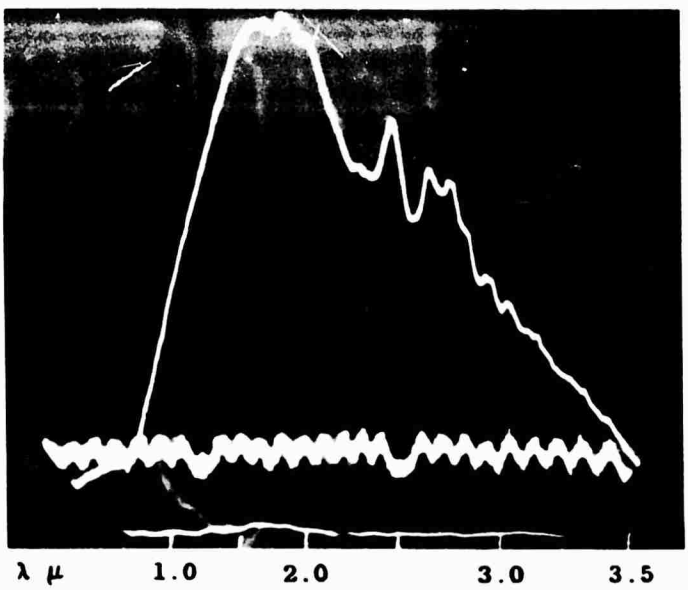

Fig. V-15 TEST 85. THE EMISSION CURVE 4.1 SEC. AFTER IGNITION.

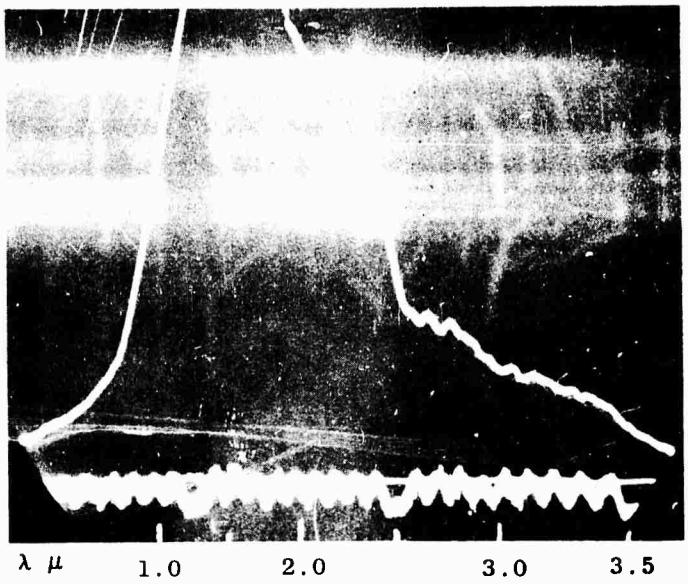

Fig. V-16 TEST 85. THE EMISSION CURVE 7.6 SEC. AFTER IGNITION.

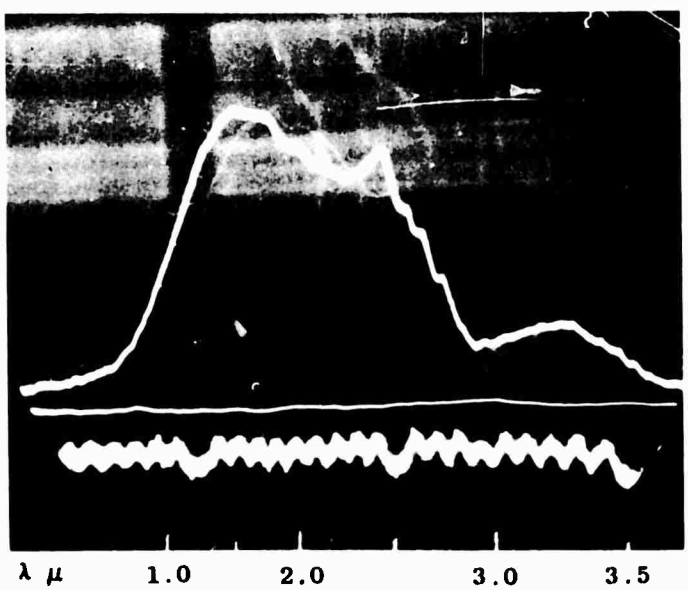

Fig. V-17 TEST 85. THE EMISSION CURVE 10.7 SEC. AFTER IGNITION.

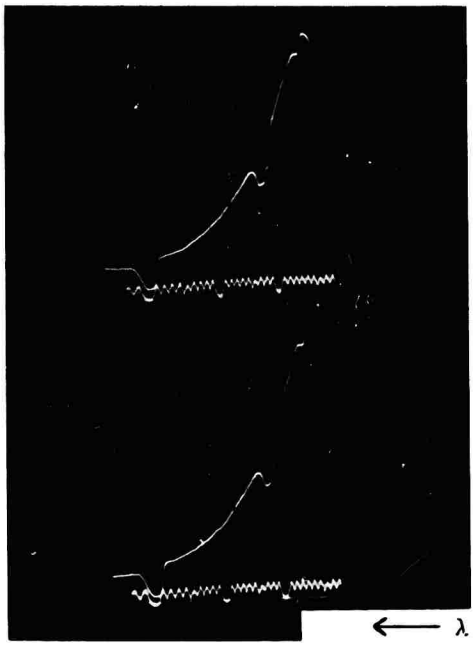

Fig. V-18

ATMOSPHERIC ABSORPTION DUE TO H_2O VAPOR AND CO_2. The source was a Nernst glower and the detector a PbTe photoconducting cell cooled to $-196^{o}C^{o}$. Note the loss of resolution due to the long time constant of the cell as compared with the upper curve in the following figure. The longer wave length sensitivity of this cell with respect to the uncooled PbSe is shown by the appearance of the 4.3μ CO_2 band at the extreme left.

Fig. V-19

ATMOSPHERIC ABSORPTION DUE TO H_2O VAPOR AND CO_2. The upper curve gives the atmospheric absorption of CO_2 and H_2O vapor using a Nernst glower source and an uncooled PbSe Photoconducting cell.

The lower curve is the same as the upper except the absorption of a thin film of polystryrene is superimposed. The 3.5μ band shows the practical limit of the PbSe detector.

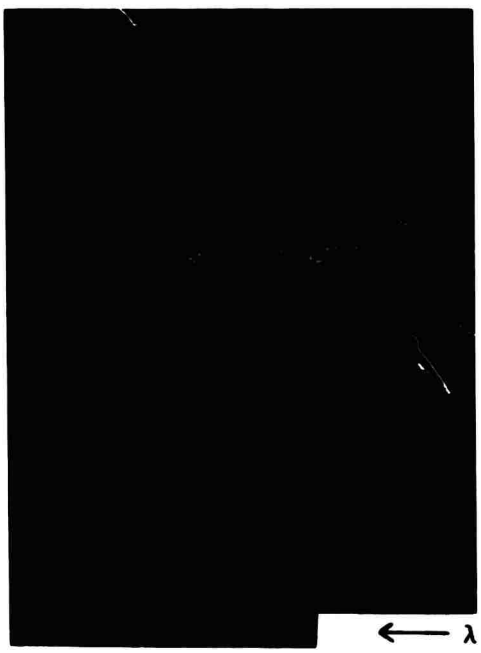

2. Test Results

Figures V-2 to V-9 are a sequence of 35mm movie pictures of Test No. 84 taken at 24 f/s with a spectrometer scanning rate of 60 cps. Each picture represents a time interval of less than 1/120 sec. A Nernst glower source was used and the effective path length in the tunnel cell was four inches. Fig. V-2 is the resultant emission curve of the glower 1/24 sec. before the ignition primer was fired, and the following figures show the resultant emission and absorption spectrum from the black powder igniter as the blast passed through the cell. Fig. V-3 shows a superposition of Figs. V-2 on the succeeding frame, and it is evident that the peak at 2.7μ is the emission spectrum of CO_2 and H_2O. The rest of the curve of Fig. V-3 is the resultant emission and absorption of CO_2, H_2O, CO and other products of the igniter explosion. The next frame, Fig. V-4, shows the recovery of the emission from the source with a small contribution from the 2.7μ emission. The emission spectrum dies out in six frames (0.25 sec) and the absorption bands increase slightly as the chamber pressure builds up to maximum.

The pressure in the absorption cell falls to about 1.5 lbs/in^2 at equilibrium which is too low for a four-inch cell path to give sufficient absorption in the wave length bandpass of this spectrometer. It is apparent that it is necessary to use the stronger absorption bands that lie at longer wave lengths. The 4.3μ CO_2 band and the 6μ H_2O band should be suitable.

In Test No. 85 a molybdenum probe was used as a radiation source for the spectrometer. This probe was placed on the axis of the test cell so the effective cell length was reduced to two inches. Fig. V-10 shows the igniter detonation with the prominent CO_2 and H_2O emission bands at 2.7μ and shorter wave lengths. The emission bands slowly died out and about a second later began

to rise again as the temperature of the probe rose. This rocket charge was excessively slow in starting to burn for some unknown reason, as shown by pressure records as well as the emission from the probe.

Succeeding spectra show that most of the radiation comes from the hot gas around the probe until its temperature gets relatively high. Emission bands are evident until the end of the run when absorption becomes noticeable.

The results from these two tests are important in that they demonstrate that the environmental difficulties, such as window fogging, vibration of the optical bench and spectrometer system and microphonics in the detection electronics, were overcome. Also, it is evident that it is necessary to extend the range of the spectrometer to include 4.3μ CO_2 and 6μ H_2O bands in order to get enough absorption to do quantitative work.

3. Equipment Modifications

Tests have recently been made with a Syracuse PbTe cell cooled to -196°C. This cell extends the range to include the 4.3μ CO_2 fundamental band, but the time constant is too long for good resolution. Fig. V-16 shows the CO_2 and H_2O atmospheric absorption bands taken with the rapid-scan spectrometer using the cooled PbTe cell. Comparing this with Fig. V-17 shows the effect of the long time constant of the cell on the resolution of the bands at 2.7μ.

Work has been started to remodel a Perkin-Elmer Model 83 monochromator to sweep at 5-10 cps and include programmed slits. This instrument will allow use of a slower response cell such as the PbTe and maintain higher resolution. Programming the slits for constant output signal versus wave length will allow wider sweep range with full sensitivity. It is planned to use this instrument with a 21-inch large screen scope so as to take advantage of the linear output of the detection system.

The new spectrometer will have a cooled PbSe cell with a sapphire window for the detector. This type cell has a response time of approximately 25μ sec and should be adequate for 10 cps scanning. However, the rapid-scan instrument will not be discarded, because its high sweep rate has many advantages with a suitable detector. It is planned to instrument this spectrometer with AuGe (P type) photovoltaic cell which, when cooled, has usable sensitivity to 8μ and a time constant less than one microsecond. This combination should be very useful for observation of transient phenomena.

Temperature Measurements

1. Principle of Operation of the APL Two-Color Pyrometer

The need for a remote control optical instrument for measuring surface temperatures of incandescent probe models and inner wall surfaces was anticipated very early in the program, and a number of experimental devices were constructed at that time. The most satisfactory arrangement of those tried proved to be a two-color ratio pyrometer utilizing a photomultiplier cell as a detector, the color sampling being accomplished by means of a rotating color filter wheel interposed in the optical path of the system. The principle of operation of the two-color ratio pyrometer depends on the fact that, for a black body radiator, the shape of the spectral curve depends only on the temperature and is given by the Planck radiation law. Therefore, the ratio of spectral densities at any two wave lengths uniquely determines the temperature, provided both points remain on the same side of the wave length corresponding to peak energy. At temperatures up to several thousand degrees Kelvin, the peak wave length appears in the infrared part of the spectrum, so that any two wave lengths in the visible region can be used in a ratio pyrometer. The present device employs narrow band interference filters centered at 5000 and 6000 Å, respectively.

The incandescent probes and innerbodies encountered in the present studies approximate black body radiators in varying degree. The shape of the spectral distribution from a smooth molybdenum cylinder, for example, does not differ from that of a true black body by amounts large enough to cause a (ratio pyrometer) temperature error of more than 5% at worst, even though the absolute light intensity is perhaps 50% off. Accuracies of 2% or better can be assured by the use of a "hohlraum", or windowed-cavity, and probes equipped with such a structure have been utilized in several tests.

2. Block Diagram and Mode of Operation

Figure V-20 shows a photograph of the APL two-color pyrometer in its present version. It consists of two parts; (1) an optical box containing the photocell, spinning filter wheel and associated optics, and (2) an instrument panel chassis connected to the optical box by means of a 75-foot, 12-conductor cable. (Cable shown in photograph is a 6-foot patch cord used for test purposes.)

Operation of the instrument is indicated in the block diagram of Fig. V-21. Light from the object whose temperature is to be measured is focused upon a calibrated field stop aperture, through which it is diffused over the sensitive area of the photocell by means of a condenser lens. The diameter of the field stop aperture determines the diameter of the spot on the test object over which temperature is to be sampled. The color wheel, driven by a synchronous motor, chops the beam, giving a 120-cycle "square wave" output from the photocell consisting of alternate "red" and "blue" pulses of equal length. This signal is then amplified in a capacitance-coupled transitorized amplifier and passed on to the main chassis via the cable. Crossed polaroids at the optical entrance to the instrument are servo-controlled to maintain either the red or blue pulse levels at constant amplitude, regardless of source temperature.

Fig. V-20 TWO-COLOR RADIATION PYROMETER: OPTICAL BOX AND MAIN CHASSIS.

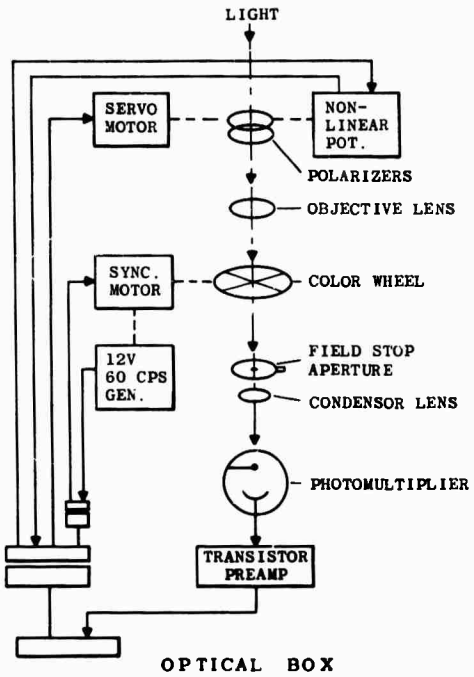

Fig. V-21 BLOCK DIAGRAM OF TWO-COLOR RADIATION PYROMETER

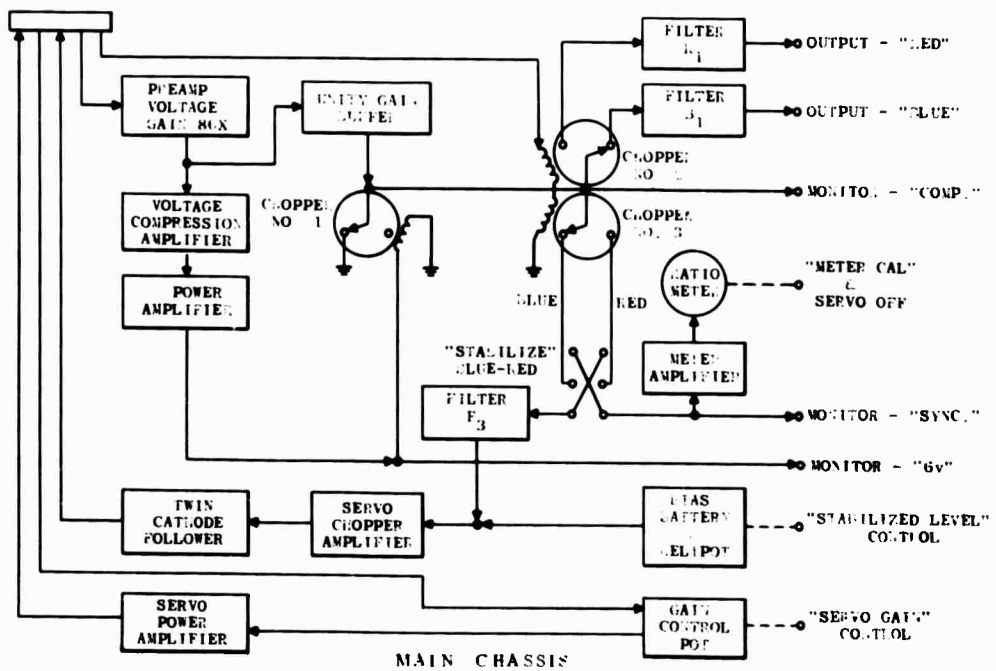

In the main chassis, the signal is further amplified to a level of two volts or less, whereupon a new "ground" reference is established by means of a chopper switch (Chopper No. 1 in Fig. V-21) which grounds the off-cycle phase of the signal 120 times a second. The driving voltage for this chopper is developed from the signal itself in order to insure synchronism, a voltage compression amplifier stage being added to isolate the driving voltage from variations in the signal amplitude. Loop instability is prevented by means of a buffer stage in the main signal path.

From this point, the 120 cps composite signal is separated into two 60 cps single-color channels by means of a second chopper switch (Chopper No. 2). To insure synchronism, the driving voltage for this chopper (as well as Chopper No. 3) is supplied by a small 60 cps generator mounted on the shaft of the color wheel motor. On account of the action of the ground reference chopper, the signals are now modulated dc rather than ac. Hence, simple RC filters of time constant 0.1 second are sufficient to convert the final red and blue 60-cycle channels to dc outputs. The twin output connectors may be seen at the lower right-hand corner of the main chassis in Fig. V-20. During an actual test run, both outputs are continuously recorded on dc oscillograph channels.

A second signal-splitting chopper (Chopper No. 3) provides the feed-back voltage to actuate the polarizer servo. An error signal is developed by comparison with an adjustable dc bias ("stabilized level" control) the setting of which determines the level of the stabilized color channel. Non-linear compensation of the error signal by means of a special pot, geared to the moving polarizer itself, is necessary to prevent instability in the servo system.

Servo gain may be adjusted at the control panel for optimum performance. A DPDT switch ("Stabilize: Blue-Red") permits selection of the color channel to be stabilized. Owing to the analogue computer action of the servo, the level of the unstabilized channel is, under static or quasistatic conditions, kept directly proportional to the color ratio and may be used to provide a single-channel measure of temperature. A panel meter is provided for this purpose. This meter indication is, of course, mainly useful in setting up the apparatus, since during an actual test run, the fluctuations in stabilized channel level are not perfectly compensated by the servo. For best accuracy, temperature should be determined from the ratio of the two dc output channels.

The three output connections at the upper right-hand corner of the instrument panel are monitor points added for convenience in trouble shooting. The terminal marked "6v" is a check point for the driving voltage of Chopper No. 1. The "sync" or synchronization terminal indicates the unstabilized color channel before filtering and is used to facilitate the adjustment of the phase relation between filter wheel and signal chopper switches. The "comp" or composite signal terminal is taken directly from the buffer amplifier and may be used as an input for a high-speed oscillograph, bypassing the RC filters, where fast response is desired.

3. Instrument Range and Calibration

The instrument is intended for use in the range 1400°K to 4000°K. The lower limit of practical operation is set by the thermal noise level in the photomultiplier tube. This could, of course, be extended by cooling the tube, though a more practical way, for a pyrometer intended primarily for measurements

at lower temperatures, would be to use a detector more sensitive at the long wave lengths. In any event, the dynamic range for a particular run is less than the total capability of the instrument, being limited by the linear range of the polarizers. This is shown in Fig. V-22, where dynamic range is indicated as a function of field stop aperture.

Calibration of the instrument is done with a standard tungsten filament lamp. Although there seems to be a certain amount of day-to-day drift in the color sensitivity of the photomultiplier, the pyrometer will hold a calibration to within an accuracy of 1% over a period of 6 hours or more The over-all accuracy in an actual temperature measurement is affected by other factors. For example, uncompensated errors due to varying spectral emissivity function of the radiating source, selective absorption in intervening windows or gas layers, etc., increase the uncertainty to several per cent.

Initial optical alignment of the pyrometer is accomplished by replacing the photomultiplier tube with a projection lamp. A fiducial spot of light is thus cast upon the object to be studied. Proper alignment is assured when this spot is correctly focused and placed in the desired location. Both the photomultiplier and projection lamp are mounted on "plug-in" units to facilitate the exchange. Current for the lamp is supplied through a 110-volt AC receptacle on the side of optical box (not visible in Fig. V-20).

4. Recent Test Data

Some recent data obtained with the pyrometer are shown in Fig. V-23. Temperatures are here plotted as a function of time from ignition for 10-second burning grains. The first figure, part A, shows the temperature history near the tip of a 3/16" molybdenum probe several inches long and supported by a strut

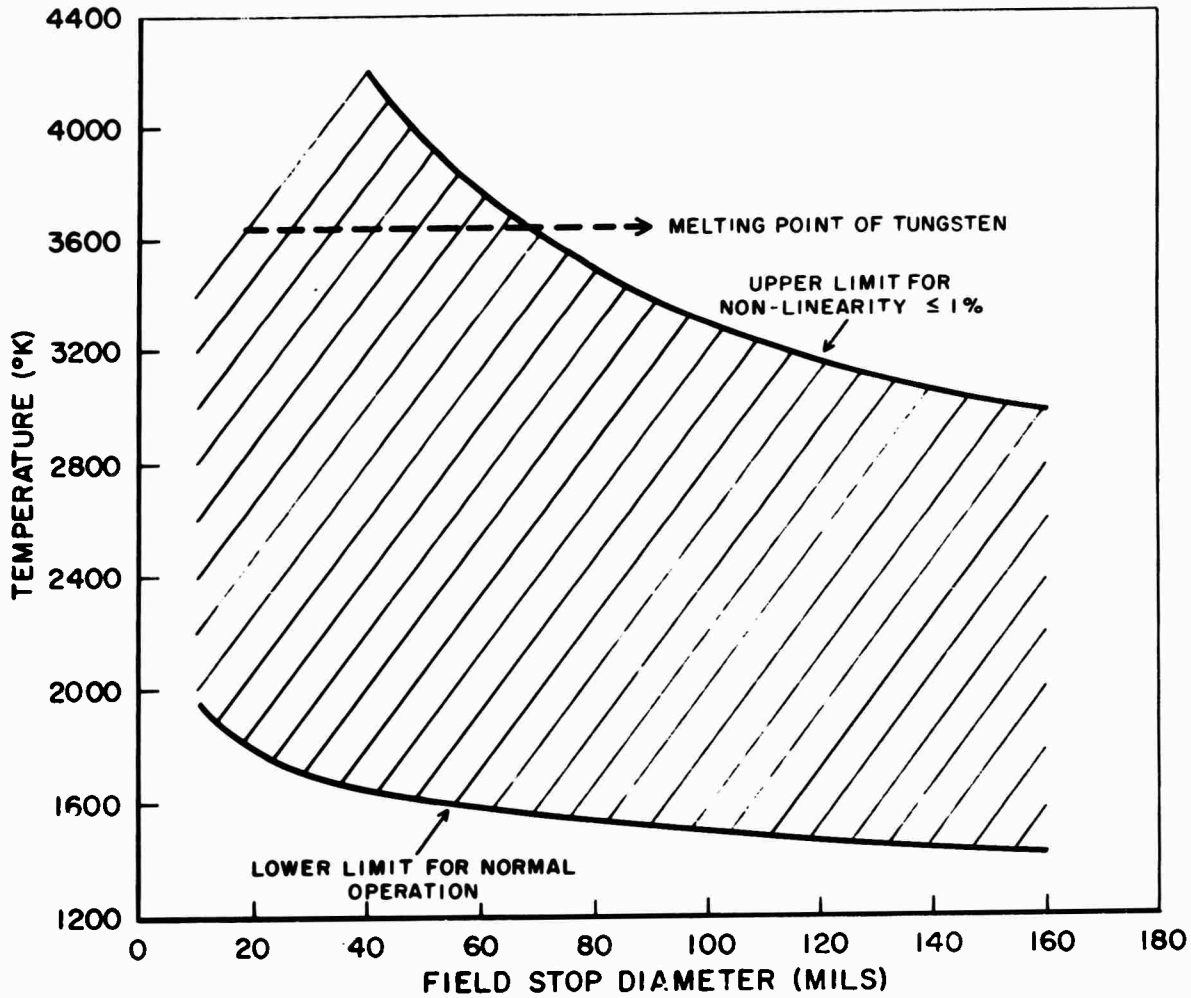

Fig. V-22 APPROXIMATE DYNAMIC RANGE FOR TWO-COLOR RADIATION PYROMETER

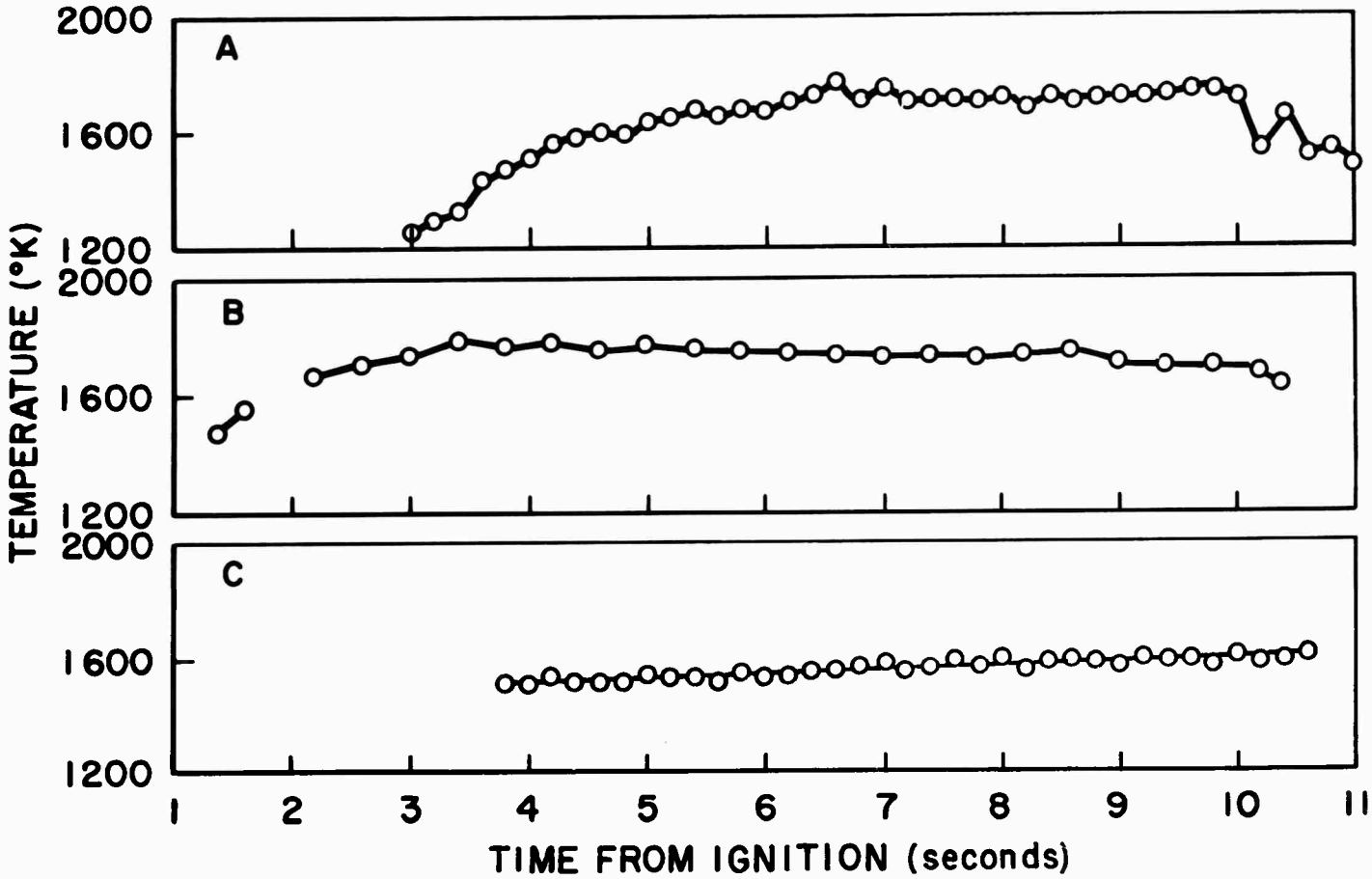

Fig. V-23 MEASURED TEMPERATURES (A) 3/16" Probe tip. B Hohlraum (C) Nozzle throat

at the rear of the four-inch test section. The field stop was set at 128 mils. It may be seen that 3-1/2 seconds were required for the temperature to rise into the calibrated range of the pyrometer (the first three points, beginning at three seconds, are extrapolations).

Figure V-23B shows the temperature as viewed through the window of a crude hohlraum placed in a position similar to that of the previous probe. The hohlraum in this case consisted of a molybdenum cup, open at the upstream end with an 80 mil x 120 mil viewing slot along the side near the base of the cavity. The cup was supported at the end of a thin one-inch long tungsten rod mounted on a strut. During alignment a 40-mil spot was placed in the downstream end of the slot. Elongation of the hohlraum window into a slot was necessary to allow room for thermal expansion of the test section.

The last plot, Fig. V-23C, shows the temperature at the nozzle throat wall. The throat wall was viewed through a 46-mil hole in the opposite wall located slightly downstream of the throat. The field stop was set up at 120 mils to collect all possible light. It was necessary to flush the viewing hole with nitrogen under high pressure in order to prevent leakage of the combustion gases. A pressure-tight quartz window sealed the outer end of the viewing hole. Calculations based on this measurement indicate an approximate heat transfer rate of 2 BTU/in^2/sec at the throat, a reasonable value for this type of rocket nozzle and propellant combination.

Facility Construction

As the number and complexity of the tests increased, it became apparent that many improvements could be made in order to facilitate assembly and alignment procedures as well as provide a greater degree of safety in the handling of

the propellant and igniter. In order to provide adequate and adjustable supports for optical equipment, such as a Schlieren apparatus, spectrometer or optical pyrometers, a pair of mobile benches were installed. These benches with table tops of 32 x 41 inches, have steel wheels and are placed on tracks which allow eight feet of motion parallel to the test section axis. These tracks, one pair on each side, have been bolted to the concrete floor. After the equipment is attached to the table tops, the benches rolled into place and the wheels locked, two fine adjustments are available for precise alignment - four inches parallel to the axis and eight inches vertically.

The new support stand for the rocket chamber, nozzle, test section, and diffuser has been designed with two point support so as to allow access completely around the nozzle and test section. The rocket combustion chamber is rigidly secured to a stand which is bolted to the concrete floor while the downstream support, located on the diffuser section, provides vertical support only via rollers to allow for thermal expansion.

The standard JATO unit used to date requires that the test section and most measuring apparatus be installed and aligned after the propellant and igniter are secured in the chamber. In order to avoid this, a new combustion chamber was designed and has been proof-tested at Allegany Ballistics Laboratory. This chamber as the closure bulkhead on the end away from the nozzle thus allowing a test to be set up completely prior to loading. An igniter which may be inserted after final assembly and alignment is also provided.

References

1. Task R Quarterly Progress Report No. 1 for the period 1 April - 30 June 1959. The Johns Hopkins University, Applied Physics Laboratory Report No. TG-331-1 (July 1959).

2. Task R Quarterly Progress Report No. 2 for the period 1 July - 30 Sept. 1959. The Johns Hopkins University, Applied Physics Laboratory Report No. TG-331-2 (October 1959).

3. Task R Quarterly Progress Report No. 3 for the period 10 October - 31 December 1959. The Johns Hopkins University, Applied Physics Laboratory Report No. TG-331-3 (January 1960).

VI. STUDY OF CONDENSED PHASE-VAPOR EQUILIBRIA

(W. E. Wilson and W. G. Berl)

Objective

Development of high specific impulse and storable propellants has led to increased interest in fuels involving metals, either as particles or as part of a more complex fuel molecule. The combustion products of metallic fuels characteristically contain a condensed phase, either as solid or liquid. In most cases the vapor pressure of the condensed substance is not known at high temperatures, nor are the equilibrium constants for reactions involving the condensed phase. The objective of this project is to develop a suitable technique of studying such equilibria under controlled laboratory conditions.

Experimental Technique

Light scattering offers a sensitive means of detecting the presence of small particles in a gas stream. By this means it should be possible to determine the onset of condensation in the hot combustion gases above a flame. The intensity of light scattered by a support flame would be monitored. Increasing amounts of a substance producing a condensable combustion product would be added. When condensation occurred there should be a large increase in the intensity of the scattered light. Since such minute amounts of particulate matter can be detected, the amount of solid would probably be a negligible proportion of the total - less than 1 per cent. (It is possible to detect 0.3μ dioctylphthlate particles at a concentration of 10^{-9} g/l.) Thus by varying the temperature of the supporting flame it should be possible to determine the vapor pressure of the condensable component. If a volatile materials were added that reacts with the condensable component, the equilibrium constant could be determined.

The B-O-H system will be studied first. At present a H_2-O_2-N_2 support flame is being used. Later a CO flame will be used to permit control of the H_2O content of the flame gases and thus permit studies of the $B_2O_3 + H_2O \rightarrow HBO_2$ reaction. A methylborate-nitrogen mixture is now being used as the B_2O_3 forming additive. Later B_2H_6 and possibly boron metal will be used.

The burner and optical system is shown in Fig. VI-1. Additional equipment includes the gas flow regulation system and a 450-cycle phase sensitive amplifier. A tungsten strip lamp is used in conjunction with a spectrometer for line reversal temperature measurements. A 100-watt mercury arc lamp is used as a light source. The scattered light is detected by a photomultiplier. The burner and optics fit into a light-tight optical housing. By suitable adjustment of the optics it is possible to measure forward scattering, or scattering at 45°, 90°, and 135°. A polarized light analyzer may be added for additional particle size measurements.

The burner is similar to one described in the literature (Ref. 1). It consists of a bundle of 0.065" stainless steel needle tubes. These are arranged in such a fashion as to form two separate flames. The inner flame will contain the condensable substance and the outer shielding flame will prevent condensation at the edges of the flame. There is provision for water cooling and an additional nitrogen shield. By using needle tubes it is possible to obtain a homogeneous column of hot gases without the difficulty of fouling by solids encountered with porous metal plate burners.

Most flames give off some visible light and the addition of boron-containing substances colors the flame green. Therefore, it is necessary to use both a filter to remove most of the light from the flame and a modulated light beam to further discriminate against non-scattered light. At present a 18A filter is placed before the photomultiplier so only the near UV mercury light is detected.

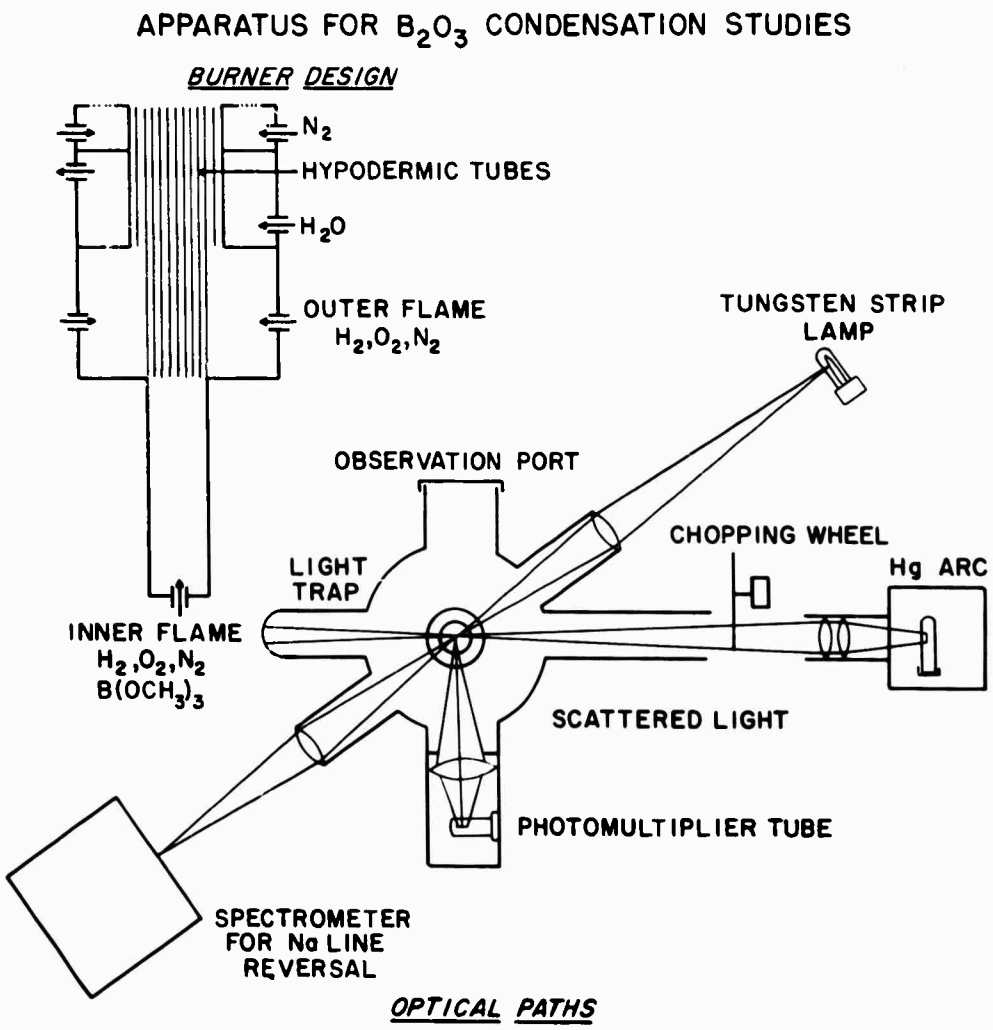

Fig. VI-1 BURNER AND OPTICAL SYSTEM FOR CONDENSATION STUDIES

Preliminary experiments indicate that the intensity of scattered light is a function of the temperature and boron content of the hot gases. The vapor pressure of boric oxide has been measured previously (Ref. 2) to 1400°K. This will provide a low temperature check and indicate whether the particles grow to sufficient size for efficient scattering, and whether supersaturation can be neglected.

References

1. C. G. James and T. M. Sugden, Proc. Roy. Soc. A248, 283 (1958).
2. J. R. Soulen, P. Sthatitanonda and J. L. Margrave, J. Phys. Chem. 59, 132 (1955).

* * * * *